Rev.Adv.Mater.Sci. 1 (2000) 27-60

NANOSCOPICS OF DISLOCATIONS AND DISCLINATIONS IN GRADIENT ELASTICITY

M. Yu. Gutkin

Institute of Problems of Mechanical Engineering, Russian Academy of Sciences,
Bolshoj 61, Vas. Ostrov, St. Petersburg 199178, Russia

Received: February 12, 2000

Abstract. The results of application of gradient theory of elasticity to a description of elastic properties of dislocations and disclinations are reviewed. The main achievement made in this approach is the elimination of the classical singularities at defect lines and the possibility of describing short-range interactions between them on a nanoscale level. Non-singular solutions for elastic fields and energies of dislocations in an infinite isotropic medium are represented in a closed analitycal form and discussed in detail. Similar solutions for straight disclinations are also considered with application to the specific case of disclination dipoles. A special attention is paid to the nanoscopic behavior and stress fields of dislocations near interfaces. Recent non-singular solutions for both the dislocation stresses and "image" forces on dislocations are demostrated in a general integral form and corresponding peculiarities in dislocation behavior near interfaces are discussed.

1. INTRODUCTION

Traditional description of elastic fields produced by dislocations and disclinations is based on the classical theory of linear elasticity [1–7]. In the isotropic case, the appropriate expressions for dislocation/disclination elastic fields are quite simple and broadly applicable to model the structure and mechanical behavior of various materials and solid state systems [1, 7–12]. However, some components of these fields are singular at the defect lines, a fact that limits the applicability of the theory to describe situations where it is important to know the strained state near defects. This concerns, for example, dislocation-disclination models for grain boundaries, as well as dislocation-disclination models simulating metallic glass structures and nanocrystalline behavior where one deals with high-density ensembles of defects. Thus, this problem is similar to that in the case of cracks [13, 14] with the well-known singular expressions predicted by classical elasticity theory.

The first attempts to modify the elastic fields of such defects within a continuum theory, were done by taking into account couple stresses [15–36]. Dislocations [15–22], disclinations [22–28] and cracks [29–36] have been considered in both Cosserat and multipolar media. The solutions found for the corresponding elastic strain and stress fields differ from the classical solutions but still possess singularities at the lines of dislocations and disclinations, as well as at the crack tips.

Following the classification given by Kunin [37], the Cosserat and multipolar media may be considered as continua having weak non-locality in elastic properties represented through a higher-order gradient of the displacement field and an additional material constant with the dimension of square length. Consideration of defects in the continua having strong non-locality, when there is an integral relation between elastic strains and stresses, gives better results – the singularities of stress fields disappear at dislocation [37–44] and disclination [44, 45] lines as well as at crack tips [41, 46, 47] but there are some hidden problems with the boundary conditions used and the convergence of the solution. It is worth noting that the most convincing solutions [37, 38] were found for dislocations in a model of quasicontinuum where the discrete structure of a solid body was taken into account. The dislocation stress fields were obtained in a closed analytical form, they were equal to zero at the dislocation line reaching extreme values at a certain distance from the dislocation line and then diminishing with small decreasing oscillations around the classical solution. To solve the same problems within a non-local continuum model with an integral relation between stresses and strains, Eringen [39–41] introduced *a priori* a special form of the kernel in the aforementioned integral relation and found other solution formulae. In the case of screw dislocations [39–41], the solutions were presented in analytical form which was reduced

Corresponding author: M. Yu. Gutkin; e-mail: gutkin@def.ipme.ru

to the classical elasticity solution when non-locality was assumed to vanish. In the case of edge dislocations [41], the solution was given in an integral form which did not allow such a limiting transition. The oscillations which were characteristic for the quasicontinuum model [37, 38], did not seem to appear here for both of these cases. It is interesting to point out that the expressions for the displacement and strain fields remained the same as in the classical theory of elasticity, with all typical singularities at the dislocation lines. Moreover, as mentioned earlier there are some problems with the number of the boundary conditions used and the convergence of the solution which, however, have not been explicitly discussed. The authors of [42–45] do not report about these peculiarities of non-local solutions though they used Eringen's model of non-local continuum.

Thus, the above non-local continuum models, among other things, can not avoid the sigularities in the displacement and strain fields. The quasicontinuum models [37, 38] avoid this difficulty, but they are hardly applicable to real materials and systems where it is necessary to account for interior and exterior boundaries, as this brings significant technical difficulties. It follows that is important to search further for non-standard continuum models which would lead to results comparable with atomistic calculations and related data of experimental observations. For example, it would be interesting to estimate the displacements and elastic strains near the defect cores and compare them with real values obtained from TEM images and related computer simulations.

We consider below another possible way to address this problem which is to use gradient modifications of the classical linear theory of elasticity. Two different gradient theories (a special one and another more general one) proposed by Aifantis and co-workers [48-56] with applications to crack problems are shortly discussed in Section 2. New non-singular solutions within the more general gradient theory of elasticity for dislocations are considered in Section 3 while those for disclinations are represented in Section 4.

2. GOVERNING EQUATIONS OF GRADIENT ELASTICITY

2.1. Special gradient theory of elasticity

In 1965, Mindlin [57] proposed a linear theory describing deformation of elastic solids where the density of strain energy was the function of strain as well as of its first and second gradients. Taking into account the second gradient of strain, the author claimed the incorporation of both cohesive forces and surface tension into the linear elasticity. The corresponding modification of Hooke's law reads [57]

$$\boldsymbol{\sigma} = \lambda(\boldsymbol{I} - c_1\boldsymbol{I}\nabla^2 - c_2\nabla\nabla)\,(\mathrm{tr}\,\boldsymbol{\varepsilon}) + 2\mu(1 - c_3\nabla^2)\boldsymbol{\varepsilon}, \quad (1)$$

where λ and μ are the usual Lamé constants, $\boldsymbol{\sigma}$ and $\boldsymbol{\varepsilon}$ denote elastic stress and strain tensors, $\boldsymbol{I}$ is the unit tensor, ∇^2 is the Laplacian; c_1, c_2 and c_3 are three independent gradient coefficients.

Substitution of (1) into the usual equilibrium equation $\nabla\cdot\boldsymbol{\sigma} = 0$ gives the following equation for the vector of displacement $\boldsymbol{u}$ [58]

$$\mu(1 - c_3\nabla^2)\nabla^2\boldsymbol{u} + \{\lambda + \mu - [\lambda(c_1 + c_2) + \mu c_3]\nabla^2\}\nabla\cdot\nabla\boldsymbol{u} = 0. \quad (2)$$

In the case, when the vector of displacement $\boldsymbol{u}$ have more than one non-vanishing components, (2) gives a system of coupled partial differencial equations which seems to be hardly solved. However, if there is the relation $c_1+c_2=c_3=c$, (2) results in

$$(1 - c\nabla^2)\{\mu\nabla^2\boldsymbol{u} + (\lambda + \mu)\nabla\nabla\cdot\boldsymbol{u}\} = 0. \quad (3)$$

In the special case when $c_1=c_3=c$ and $c_2=0$, Eq. 1 transforms into

$$\boldsymbol{\sigma} = \lambda(\mathrm{tr}\,\boldsymbol{\varepsilon})\boldsymbol{I} + 2\mu\boldsymbol{\varepsilon} - c\nabla^2[\lambda(\mathrm{tr}\,\boldsymbol{\varepsilon})\boldsymbol{I} + 2\mu\boldsymbol{\varepsilon}]. \quad (4)$$

Namely this equation was initially proposed by Altan and Aifantis [48] to eliminate the strain singularity at the mode-III crack tip. They also showed that for an atomic lattice, the gradient coefficient c can be estimated [48] as $\sqrt{c} \approx a/4$, where a is the lattice constant. Substitution of (4) into the equilibrium equation $\nabla\cdot\boldsymbol{\sigma} = 0$ leads again to (3). A physical derivation of (3) and (4) based on a mixture-like model for composite materials was provided by Aifantis [50] and later in more detail by Altan and Aifantis [54]. Ru and Aifantis [49] have found a simplified way to solve boundary-value problems in this special theory of gradient elasticity described by (3) or (4), by reducing them to solving a non-homogeneous Helmholtz equation with the "source" term given in terms of well-known solutions for the same problems in classical elasticity. They have also shown that the stress field in this theory of gradient elasticity remains the same as in classical elasticity. Altan and Aifantis [54] have used a Fourier transform procedure to solve (3) in two dimensions including the mode-I and -II cracks problems.

Application of this theory to crack problems has resulted [48–54] into the elimination of the classical singularities from the solutions for the elastic displacement and strain fields at the crack tips. The stress components, however, remained as in the classical theory but this difficulty has been considered as less

severe than the strain singularity because the stress may not be rigorously defined at the atomic level near a discontinuity.

Encouraged by these results, we applied the special gradient elasticity theory given by (4) to dislocations [59, 60] and disclinations [58]. As was the case with cracks, new gradient solutions for displacement [59, 60], strain fields [59, 60] and energies [58] of dislocations as well as for strain fields [58] of disclinations were non-singular at the defect lines. The corresponding stress fields were the same as in the classical theory of elasticity.

2.2. More general gradient theory of elasticity

In unpublished work by Ru and Aifantis [55] (see also [56]) a simple extension of the gradient elasticity model given by (4) was used to dispense with both strain and stress singularity at the dislocation core and at the crack tip. The constitutive equation of this theory reads

$$(1-c_1\nabla^2)\boldsymbol{\sigma} = (1-c_2\nabla^2)[\lambda(\mathrm{tr}\,\boldsymbol{\varepsilon})\boldsymbol{I} + 2\mu\boldsymbol{\varepsilon}], \tag{5}$$

with two different gradient coefficients c_1 and c_2. In [55] a rather simple mathematical procedure analogous to the one contained in [49] has been outlined for the solution of (5) in terms of solutions of classical elasticity for the same boundary-value problem. In fact, it is easily established (see [49], also [58-60]) that the right hand side of (5) for the case of $c_1 \equiv 0$, gives the classical solution for the stress field which we denote here by $\boldsymbol{\sigma}^0$, while the solution for the displacement is determined through the inhomogeneous Helmholtz equation given by

$$(1-c_2\nabla^2)\boldsymbol{u} = \boldsymbol{u}^0, \tag{6}$$

where $\boldsymbol{u}^0$ denotes the solution of classical elasticity for the same traction boundary-value problem. Equation (6) implies a similar equation for strain $\boldsymbol{\varepsilon}$ of the gradient theory

$$(1-c_2\nabla^2)\boldsymbol{\varepsilon} = \boldsymbol{\varepsilon}^0, \tag{7}$$

in terms of the strain $\boldsymbol{\varepsilon}^0$ of the classical elasticity theory for the same traction boundary-value problem. With the displacement or strain field thus determined (which is obviously independent of whether $c_1 \equiv 0$ or $c_1 \neq 0$), it follows that the stress field $\boldsymbol{\sigma}$ of (5) can be determined (for the case $c_1 \neq 0$) from the equation

$$(1-c_1\nabla^2)\boldsymbol{\sigma} = \boldsymbol{\sigma}^0, \tag{8}$$

where $\boldsymbol{\sigma}^0$ denotes the solution obtained for the same boundary-value problem within the classical theory of elasticity.

Thus, in order to solve equation (5), one can solve separately equations (7) and (8) by utilizing the classical solutions $\boldsymbol{\varepsilon}^0$ and $\boldsymbol{\sigma}^0$ provided that appropriate care is taken for the extra (due to the higher order terms) boundary conditions or conditions at infinity. For dislocations and disclinations in a homogeneous medium, this problem solutions are accounted for by assuming that the strain and stress fields at infinity are the same for both the gradient and classical theory. The approach has firstly been applied [55] to the cases of screw dislocations and mode-III cracks where the asymptotic solutions at the dislocation line and crack tip have been found demonstrating the elimination of both strain and stress singularities there. Recently, the gradient elasticity described by (5) has been used to find nonsingular solutions for stress fields of dislocations [61, 62] and disclinations [62, 63] in homogeneous solid. The boundary-value problems of dislocations near interfaces within the gradient elasticity theory (5) have been solved in [64–66] where non-singular expressions have been found for dislocation stress fields as well as for "image" forces on dislocations due to interfaces.

3. NANOSCALE ELASTIC PROPERTIES OF DISLOCATIONS

3.1. Straight dislocations in homogeneous media

3.1.1. A general solution

Consider a mixed dislocation whose line coincides with the *z*-axis of a Cartesian coordinate system. Let it's Burgers vector be $\boldsymbol{b}=b_x\boldsymbol{e}_x+b_z\boldsymbol{e}_z$ thus determining the edge (b_x) and screw (b_z) components.

Classical solution

In the framework of classical elasticity theory, the total displacement field is described by

$$\boldsymbol{u}^0 = \frac{b_x\boldsymbol{e}_x + b_z\boldsymbol{e}_z}{2\pi}\left\{\arctan\frac{y}{x} + \frac{\pi}{2}\,\mathrm{sign}(y)[1-\mathrm{sign}(x)]\right\} + \frac{b_x}{4\pi(1-\nu)}\left\{\boldsymbol{e}_x\frac{xy}{r^2} - \boldsymbol{e}_y\left[(1-2\nu)\ln r + \frac{x^2}{r^2}\right]\right\}, \tag{9}$$

where ν is the Poisson ratio, $r^2=x^2+y^2$. Here we use a single-valued discontinuous form suggested by de Wit [5]. The elastic strain field ε_{ij}^0 reads (in units of $1/[4\pi(1-\nu)]$) by [1, 5]

$$\begin{aligned}
\varepsilon_{xx}^0 &= -b_x y[(1-2\nu)r^2 + 2x^2]/r^4,\\
\varepsilon_{yy}^0 &= -b_x y[(1-2\nu)r^2 - 2x^2]/r^4,\\
\varepsilon_{xy}^0 &= b_x x(x^2-y^2)/r^4,
\end{aligned} \tag{10}$$

$$\varepsilon^0_{xz} = -b_z(1-\nu)y/r^2,$$
$$\varepsilon^0_{yz} = b_z(1-\nu)x/r^2,$$

and the elastic stress field σ^0_{ij} is (in units of $\mu/[2\pi(1-\nu)]$) [1, 5]

$$\begin{aligned}
&\sigma^0_{xx} = \varepsilon^0_{xx}(\nu=0),\\
&\sigma^0_{yy} = \varepsilon^0_{yy}(\nu=0),\\
&\sigma^0_{zz} = \nu(\sigma^0_{xx}+\sigma^0_{yy}),\\
&\sigma^0_{xy} = \varepsilon^0_{xy},\\
&\sigma^0_{xz} = \varepsilon^0_{xz},\\
&\sigma^0_{yz} = \varepsilon^0_{yz}.
\end{aligned} \tag{11}$$

Fields (9) (*y*-component), (10) and (11) are singular at the dislocation line.

The elastic energy W^0 of the dislocation per unit dislocation length is [1]

$$W^0 = \frac{\mu}{4\pi}\left(b_z^2 + \frac{b_x^2}{1-\nu}\right)\ln\frac{R}{r_0}, \tag{12}$$

where R denotes the size of the solid and r_0 is a cut-off radius for the dislocation elastic field near the dislocation line. When $r_0 \to 0$, W^0 becomes singular.

Gradient solution

Let us now consider the corresponding dislocation fields within the theory of gradient elasticity given by (5). As described in Section 2.2, one can obtain the solution of (5) by solving separately equations (6)–(8). They can be solved [58, 60–66] by using the Fourier transform method. Omitting intermediate calculations, we give here only the final results. For the total displacements, solution of (6) gives [59, 60–62]

$$\begin{aligned}
\boldsymbol{u} = \boldsymbol{u}^0 &- \frac{b_x}{4\pi(1-\nu)}\{[\boldsymbol{e}_x 2xy + \boldsymbol{e}_y(y^2 - x^2)]r^2\boldsymbol{\Phi}_2 + \boldsymbol{e}_y\boldsymbol{\Phi}_0\} + \frac{b_x\boldsymbol{e}_x + b_z\boldsymbol{e}_z}{2\pi}\,\mathrm{sign}(y)\\
&\times\int_0^{+\infty}\frac{s\sin(sx)}{\frac{1}{c_2}+s^2}\,e^{-|y|\sqrt{\frac{1}{c_2}+s^2}}\,ds,
\end{aligned} \tag{13}$$

where $\boldsymbol{u}^0$ is given by (9), $\Phi_0 = (1-2\nu)K_0(r/\sqrt{c_2})$, $\Phi_2 = [2c_2/r^2 - K_2(r/\sqrt{c_2})]/r^4$, $K_n(r/\sqrt{c_2})$ is the modified Bessel function of the second kind and n=0,1, … denotes the order of this function.

For the elastic strain, solution of (7) gives [59, 60–62] $\varepsilon_{ij} = \varepsilon^0_{ij} + \varepsilon^{gr}_{ij}$ where ε^0_{ij} are given by (10) and ε^{gr}_{ij} (in units of $1/[2\pi(1-\nu)]$) by

$$\begin{aligned}
&\varepsilon^{gr}_{xx} = b_x y[(y^2-\nu r^2)\Phi_1 + (3x^2-y^2)\Phi_2],\\
&\varepsilon^{gr}_{yy} = b_x y[(x^2-\nu r^2)\Phi_1 - (3x^2-y^2)\Phi_2],\\
&\varepsilon^{gr}_{xy} = -b_x x[y^2\Phi_1 + (x^2-3y^2)\Phi_2],\\
&\varepsilon^{gr}_{xz} = b_z(1-\nu)yr^2\Phi_1/2,\\
&\varepsilon^{gr}_{yz} = -b_z(1-\nu)xr^2\Phi_1/2,
\end{aligned} \tag{14}$$

where $\Phi_1 = K_1(r/\sqrt{c_2})/(\sqrt{c_2}r^3)$. For the stresses, the solution of (8) gives [61, 62] $\sigma_{ij} = \sigma^0_{ij} + \sigma^{gr}_{ij}$, where σ^0_{ij} are given by (11) and σ^{gr}_{ij} (in units of $\mu/[\pi(1-\nu)]$) by

$$\begin{aligned}
&\sigma^{gr}_{xx} = \varepsilon^{gr}_{xx}(\nu=0, c_2 \leftrightarrow c_1),\\
&\sigma^{gr}_{yy} = \varepsilon^{gr}_{yy}(\nu=0, c_2 \leftrightarrow c_1),\\
&\sigma^{gr}_{zz} = \nu(\sigma^{gr}_{xx}+\sigma^{gr}_{yy}),\\
&\sigma^{gr}_{xy} = \varepsilon^{gr}_{xy}(c_2 \leftrightarrow c_1),\\
&\sigma^{gr}_{xz} = \varepsilon^{gr}_{xz}(c_2 \leftrightarrow c_1),\\
&\sigma^{gr}_{yz} = \varepsilon^{gr}_{yz}(c_2 \leftrightarrow c_1).
\end{aligned} \tag{15}$$

The main feature of the solution given by (13)–(15) is the absence of any singularities in the displacement, strain and stress fields. In fact, when $r \to 0$, we have $K_0(r/\sqrt{c_k})|_{r\to 0} \to -\gamma + \ln(2\sqrt{c_k}/r)$, $K_1(r/\sqrt{c_k}) \to \sqrt{c_k}/r$, $K_2(r/\sqrt{c_k}) \to 2c_k/r^2 - 1/2$, ($k$=1,2), γ =0.57721566… is Euler's constant and, thus, u_y is finite, $\varepsilon_{ij} \to 0$, $\sigma_{ij} \to 0$. The fields of displacements (13) and strains (14) have been analysed in detail in [59, 60] within a special version of gradient elasticity theory ($c_1 \equiv 0$). The stress fields (15) have been examined in [61]. We discuss below the main features of (13)–(15) separately for screw (Section 3.1.2*)* and edge (Section 3.1.3*)* dislocations.

Using (15), one can find the elastic energy of the dislocation within the gradient elasticity given by (5) as the work $W_s = -\frac{1}{2}\int_V \sigma_{zy}\beta^{*(cl)}_{yz}dV$ (for screw dislocations) and $W_e = -\frac{1}{2}\int_V \sigma_{xy}\beta^{*(cl)}_{yx}dV$ (for edge dislocations) done by the gradient-dependent dislocation stress field (15) for producing the corresponding classical (for simplicity) plastic distortion $\beta^{*(cl)}_{yi} = (b_i/2)\delta(y)[1-\mathrm{sign}(x)]$, i=x,z [5]. The final result reads [61]

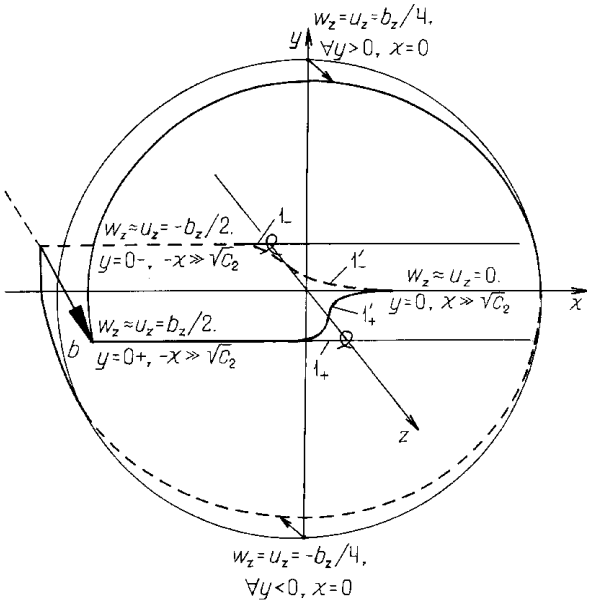

Fig. 1. Total displacements around a screw dislocation in an infinite body. The curves $1_{\pm}$ and $1'_{\pm}$ denote schematically respectively the profiles of total displacements $u_z(x,y=0_{\pm})$ for the classical solution and $w_z(x,y=0_{\pm})$ for the gradient solution along the plane $y=0$.

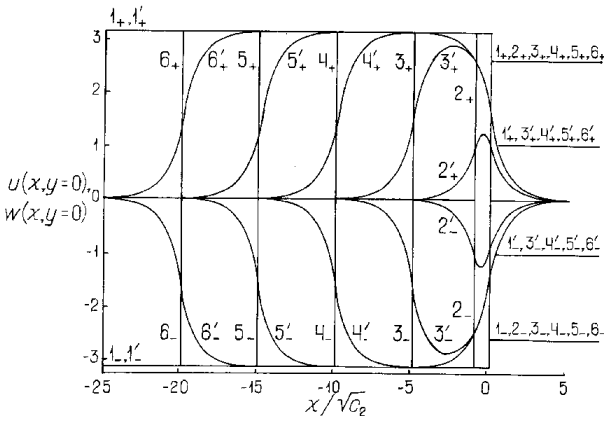

Fig. 2. The profiles of total displacements for a separate screw dislocation ($1_{\pm}$ — classical solution, and $1'_{\pm}$ — gradient solution) and for a dislocation dipole with arm d ($2_{\pm}$—$6_{\pm}$ — classical solution, and $2'_{\pm}$—$6'_{\pm}$ - gradient solution). The ratio $d/\sqrt{c_2}$ is taken as $\infty(1_{\pm},1'_{\pm})$, 1 ($2_{\pm},2'_{\pm}$), 5 ($3_{\pm},3'_{\pm}$), 10 ($4_{\pm},4'_{\pm}$), 15 ($5_{\pm},5'_{\pm}$), and 20 ($6_{\pm},6'_{\pm}$).

$$W = \frac{\mu}{4\pi(1-\nu)}\left\{\frac{b_x^2}{2} + [b_x^2 + (1-\nu)b_z^2]\left(\gamma + \ln\frac{R}{2\sqrt{c_1}}\right)\right\}. \qquad (16)$$

Thus, we obtain a strain energy expression which is not singular at the dislocation line.

It is worth noting [58] that the energy expression (16) contains only one gradient coefficient c_1 that looks strangely. A more general consideration would include also the corresponding gradient expressions for the plastic distortions (e.g. $\beta^{*(gr)}_{yz} = (b_z/2)\delta(y)[1-\mathrm{sign}(x)](1-e^{-|x|/\sqrt{c_2}})$ given in [59] for screw dislocation). The resultant energy expressions $W_s = -\frac{1}{2}\int_V \sigma_{zy}\beta^{*(gr)}_{yz}dV$ (screw) and $W_e = -\frac{1}{2}\int_V \sigma_{xy}\beta^{*(gr)}_{yx}dV$ (edge) would contain now both gradient coefficients c_1 and c_2.

3.1.2. Screw dislocations

Consider a screw dislocation whose line coincides with the z-axis of a Carthesian coordinate system (Fig. 1) and discuss briefly the main most interesting features [59, 61] of the gradient solution for dislocation fields (13)–(15) which distinguish it from the well-known classical solution (9)–(11).

First, let us compare the behavior of total displacements (9) and (13) on the "cutting" plane y=0. In the case of the screw dislocation (Fig. 1), the displacement vector has the only non-vanishing component $w_z = b_z/(2\pi)w(x,y)$. When $y \to 0$, the integral in (13) may be evaluated in an explicit form [59] that gives

$$w(x, y \to 0) = \frac{\pi}{2}\mathrm{sign}(y)\left[1 - \mathrm{sign}(x)\left(1 - e^{-\frac{|x|}{\sqrt{c_2}}}\right)\right]. \qquad (17)$$

The additional term "$-e^{-\frac{|x|}{\sqrt{c_2}}}$" which appears in the gradient solution (17) leads to the smoothing of the total displacement profiles (curves $1'_+$ and $1'_-$ in Figs. 1 and 2), in contrast to the abrupt jumps occuring in these profiles in the classical solution (curves 1_+ and 1_- in Figs. 1 and 2). It is interesting to note that the size of such a transition zone is approximately $10\sqrt{c_2}$ which gives the value 2.5a for a crystalline lattice, i.e. the usual size of the dislocation core. It follows that in gradient elasticity, the dislocation core appears naturally as a result of a calculation defining the region of maximum strain around the dislocation line [59]. In classical elasticity, there is no definition for the dislocation core and the dislocation is treated as a linear singularity of elastic stress and strain fields.

Second, it is interesting to compare the displacement field (17) with the corresponding field derived within a model accounting for the atomic structure of

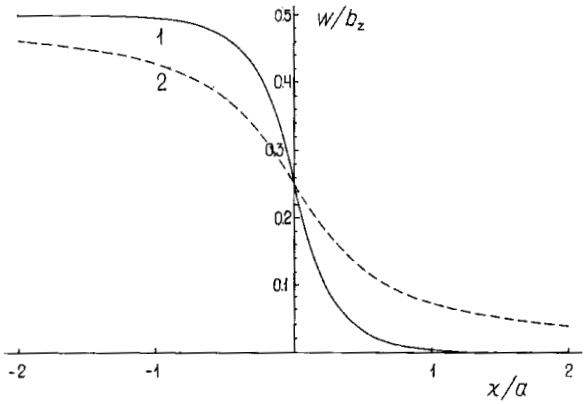

Fig. 3. Total displacements near the line of screw dislocation within the gradient model (1) and the Peierls-Nabarro model (2) when $y \to +0$.

a solid body [58]. In particular, we consider the Peierls-Nabarro dislocation model [1] which in our case gives the following expression for the total displacement $w_z^{(PN)}$ at $y \to 0$

$$w_z^{(PN)}(x, y \to 0) = \frac{b_z}{2\pi}\,\mathrm{sign}(y)\left(\frac{\pi}{2} - \arctan\frac{x}{a/2}\right), \quad (18)$$

where a is the lattice constant. Using the estimate $\sqrt{c_2} \approx a/4$ [48, 50], we depict graphically (17) and (18) in Fig. 3. One can conclude that the gradient model gives much narrower dislocation core (about $2a$) than the Peierls-Nabarro model.

Let us consider now a gradient solution for a dipole of screw dislocations [59]. As usually, such a solution may be found simply by a superposition of solutions for separate dislocations. The only reason for discussing this case here is due to a new interesting effect concerning the behavior of the total displacement of a dipole. Consider two parallel screw dislocations lying in the plane $y=0$ along the z-axis and crossing the x-axis at the points $x=-d$ and $x=0$. Let us assume the same Burgers vector b_z and opposite tangent vectors $\pm l_z$. This means that they can be treated as a limiting case of a rectangular gliding dislocation loop having edge segments at $z=\pm\infty$. In the framework of classical dislocation theory, the field of total displacement for such a dislocation configuration is described by the vector $u_z=b_z/(2\pi)u(x,y)$, where

$$u(x, y) = \arctan\frac{y}{x} - \arctan\frac{y}{x+d} + \frac{\pi}{2}\,\mathrm{sign}(y)[\mathrm{sign}(x+d) - \mathrm{sign}(x)]. \quad (19)$$

The gradient solution is described by the vector $w_z=b_z/(2\pi)w(x,y)$, where

$$w(x, y) = u(x, y) - \mathrm{sign}(y)\frac{i}{2}\int_{-\infty}^{+\infty}(1 - e^{ids})\frac{s}{\frac{1}{c_2} + s^2}\,e^{-|y|\sqrt{\frac{1}{c_2}+s^2}}\,e^{isx}\,ds, \quad (20)$$

and $u(x,y)$ is given by (19).

When $y \to 0$,

$$w(x, y \to 0) = \frac{\pi}{2}\,\mathrm{sign}(y)\left[\mathrm{sign}(x+d)\left(1 - e^{-\frac{|x+d|}{\sqrt{c_2}}}\right) - \mathrm{sign}(x)\left(1 - e^{-\frac{|x|}{\sqrt{c_2}}}\right)\right]. \quad (21)$$

The graphs for $u(x,y\to 0)$ and $w(x,y\to 0)$ are presented in Fig. 2. Besides the evident difference in the form of these profiles, it is important to note that the maximum value of the total displacement depend on the dipole arm d for the gradient solution w, in contrast to the classical solution u which is independent of d. This dependence disappears when $d \ge d_0 \approx 10\sqrt{c_2}$ where d_0 defines a new characteristic distance; namely, the radius of the "strong short-range interaction" between dislocations. This gives $d_0 \approx 2a$, a result consistent with intuition.

As it has been pointed out in Section 3.1.1, the main feature of the gradient solution given by (14) and (15) is the absence of any singularities in both the strain and stress fields (previous models eliminated eather the strain or stress singularity but not both, see Section 1). It is interesting to note that the stress components σ_{xz} and σ_{yz} given by the superpositions of corresponding components in (11) and (15), are exactly the same as the ones obtained by Eringen [39-41] for the stress field of a screw dislocation within his version of non-local elastisity. To illustrate the characteristic features of the gradient solution, the spatial distribution of elastic strains ε_{iz} and stresses σ_{iz} ($i=x,y$) near the dislocation line [58, 61] is presented in Fig. 4. One can see that the gradient solutions for the elastic strains and stresses attain their extreme values of approximately $\pm b_z/(10\pi\sqrt{c_2})$ and $\pm\mu b_z/(5\pi\sqrt{c_1})$ at a distance $\approx\sqrt{c_2}$ and $\sqrt{c_1}$ from the dislocation line, respectively. Using for the gradient coefficients c_1 and c_2 the estimate [48, 50] $\sqrt{c_1} \approx \sqrt{c_2} \approx a/4$ for a crystalline lattice, we find that $\max|\varepsilon_{iz}| \approx 12\%$ [59] and $\max|\sigma_{iz}| \approx \mu/4$ [61] at a distance $\approx a/4$ from the dislocation line. It is also seen that the gradient solutions coincide with the

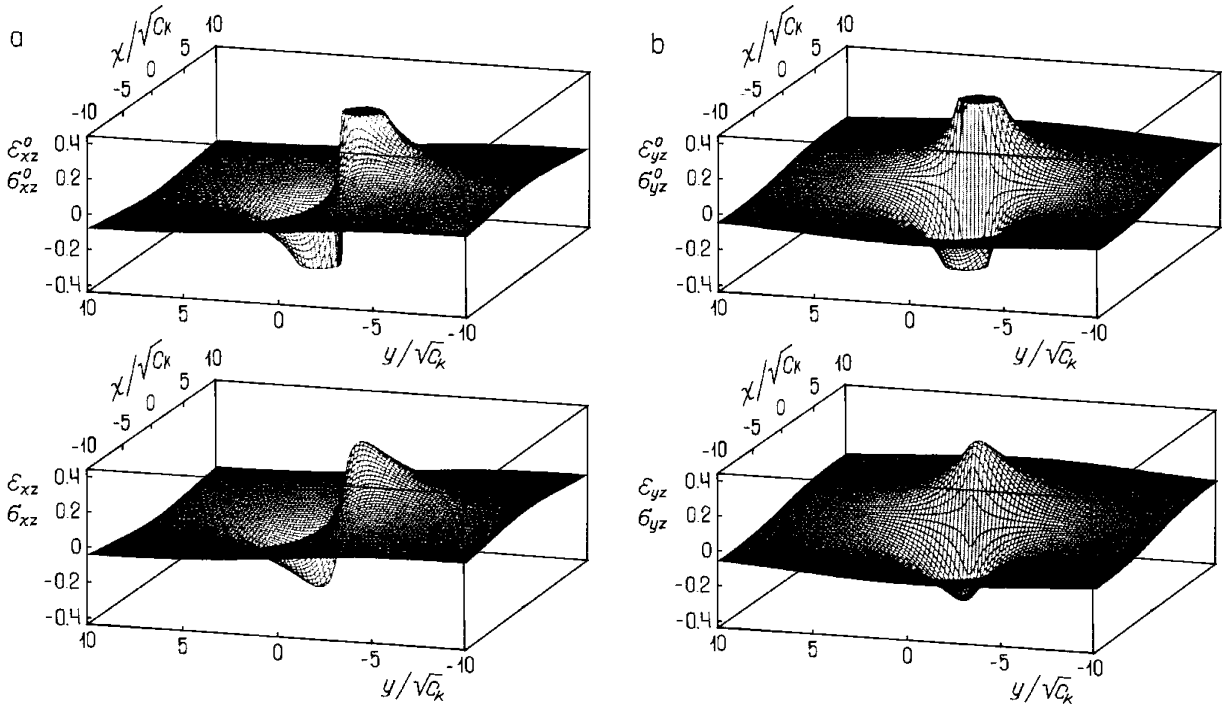

Fig. 4. The coordinate-depended parts of strain ε^0_{xz}, ε_{xz} – (a), ε^0_{yz}, ε_{yz} – (b), or stress σ^0_{xz}, σ_{xz} – (a), σ^0_{yz}, σ_{yz} – (b) components near the line of a screw dislocation which goes through the point $(0,0)$. The strain values are given in units of $b_z/(4\pi\sqrt{c_2})$ while the stress values in units of $\mu b_z/(2\pi\sqrt{c_1})$. The top figures give the classical solutions ε^0_{iz}, σ^0_{iz} while the bottom ones give the gradient solution ε_{iz}, σ_{iz}, $(i=x,y)$.

classical ones far away from the dislocation core $(r \geq r_0 \approx 4\sqrt{c_k})$ [59].

The elimination of singularity from the strain and stress fields permits us to consider in detail the short-range nanoscale interaction between dislocations. It has been shown above that such short-range interaction takes place when the spacing d between dislocations is smaller than $\approx 10\sqrt{c_2} \approx 2.5a$. Here we consider two simple dislocation configurations: a dipole and a pair of screw dislocations (Fig. 5) [58]. The elastic fields of these configurations are obtained as simple superpositions of the corresponding fields for individual dislocations. Fig. 6 shows the distribution of the strain and stress components, $\varepsilon_{yz}(x,0)$ and $\sigma_{yz}(x,0)$, near the dislocation dipole (Fig.6 a,b) and dislocation pair (Fig. 6 c,d). One can see that the strain and stress are finite at the dislocation lines and tend to zero there when the magnitude of interdislocation spacing d increases. Between dislocations or near them, where the classical solutions (dashed curves) give unreasonably high strain and stress values, the gradient solutions (solid curves) give quite reasonable values, $\varepsilon_{yz} \leq 25\%$ and $\sigma_{yz} \leq \mu/2$. In the case of dislocation dipoles, the strain and stress at the central point between the dislocations do not exceed these levels and tend to zero when $d \to 0$ (Fig. 7). In the case of a dislocation pair, the levels of strain and stress decrease between the dislocation lines as they glide to each other and remain finite all the way up to the point where the two dislocations come together at the same line. We can conclude [58] that the short-range elastic interaction between dislocations is much smaller than that predicted from classical elasticity. This means that there is no significant energetic barriers for the processes of elementary nucleation of dislocation dipoles or formation of superdislocations in high-density dislocation ensembles where the interdislocation spacing is of the order of a few nanometers.

3.1.3. Edge dislocations

Consider an edge dislocation whose line coinsides with the z-axis while the Burgers vector $\boldsymbol{b}=b_x\boldsymbol{e}_x$ is parallel to the x-axis of the Carthesian coordinate system. The most interesting question here is the behavior of the total displacement and elastic strain and stress near the dislocation line [60, 61].

First, consider the components u_x and u_y of the total displacement given by (13), on the "cutting plane" $y=0$. When $y \to 0$, we have [60]

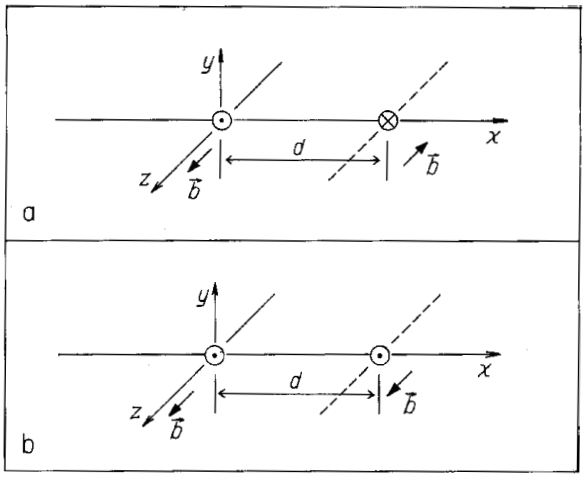

Fig. 5. The dipole (a) and pair (b) of screw dislocations.

$$u_x(x, y \to 0) = \frac{b_x}{4}\,\mathrm{sign}(y) \times\left[1-\mathrm{sign}(x)\left(1-e^{-\frac{|x|}{\sqrt{c_2}}}\right)\right], \tag{22}$$

$$u_y(x, y \to 0) = \frac{b_x}{4\pi(1-\nu)}\left[-1-(1-2\nu)\ln|x|+\frac{2c_2}{x^2} -(1-2\nu)K_0\left(\frac{|x|}{\sqrt{c_2}}\right)-K_2\left(\frac{|x|}{\sqrt{c_2}}\right)\right]. \tag{23}$$

Expression (22) coincides with Eq. (17) which describes the total displacement of a screw dislocation at y=0. The term "$-e^{-\frac{|x|}{\sqrt{c_2}}}$" which appears in the gradient solution (22) leads to the smoothing of the total displacement profile in contrast to the abrupt jump occuring in this profile in the classical solution (see Figs. 1 and 2). This means that in gradient elasticity, the dislocation core appears again naturally, directly from the calculations as we have discussed this above for the screw dislocation.

Expression (23) contains the terms which are singular at the dislocation line. However, they compensate each other. To demonstrate this correctly, let us consider here the field of total displacements created by a dipole of edge dislocations, thus avoiding the logarithm of dimensional quantity.

Let two parallel edge dislocations lie in the plane y=0 along the z-axis and cross the x-axis at the points x=-d and x=0. Let us assume the same Burgers vector b_x and opposite tangent vectors $\pm l_z$. This means that they can be treated as a limiting case of a rectangular gliding dislocation loop having screw segments at

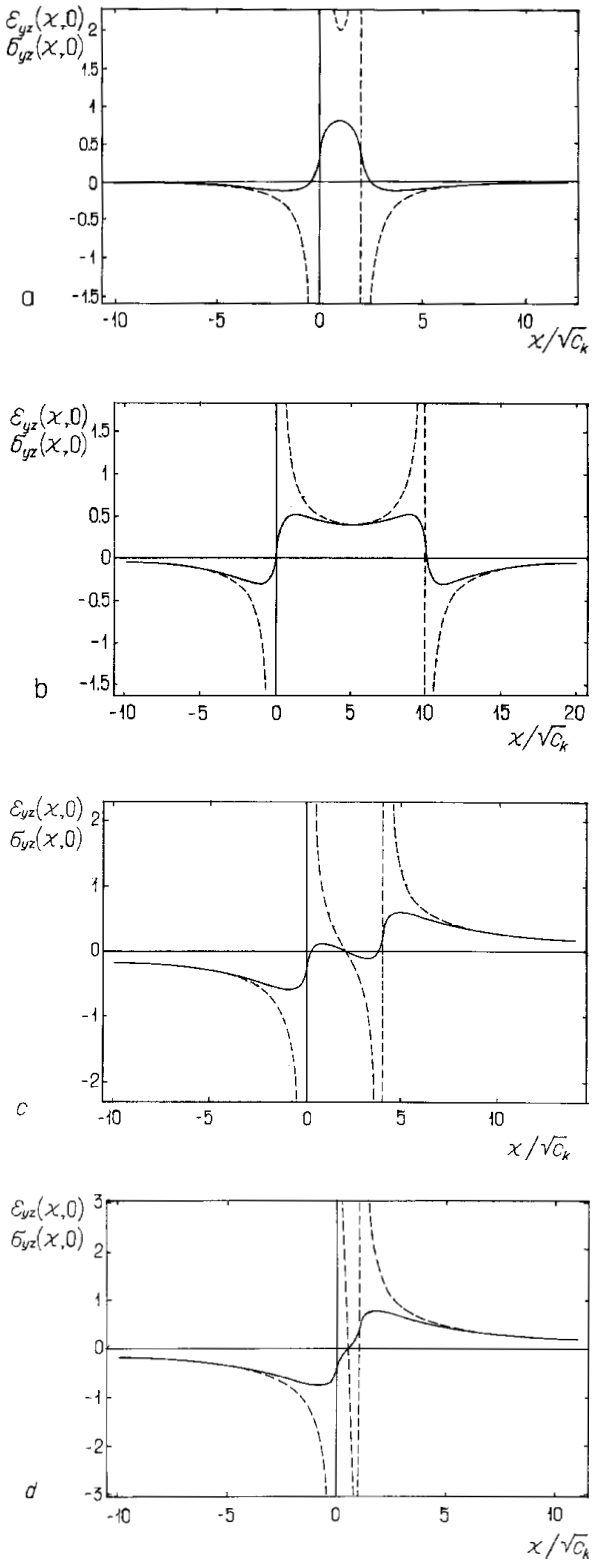

Fig. 6. The coordinate-depended parts of strain $\varepsilon_{yz}(x,0)$ or stress $\sigma_{yz}(x,0)$ near the dipole (a,b) and pair (c,d) of screw dislocations for different values of the interdislocation spacing $d/\sqrt{c_k}$ =2 (a), 10 (b), 4 (c), and 1(d), where k=2 corresponds to strain distribution while k=1 to stress distribution. The strain values are given in units of $b_z/(4\pi\sqrt{c_2})$ while the stress values in units of $\mu b_z/(2\pi\sqrt{c_1})$. The dashed curves represent the classical solution.

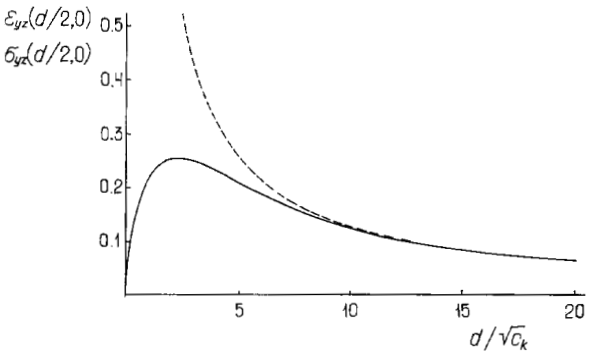

Fig. 7. The strain and stress components, $\varepsilon_{yz}(d/2,0)$ and $\sigma_{yz}(d/2,0)/(2\mu)$, in the middle of the dipole of screw dislocations via the dipole arm $d/\sqrt{c_k}$ for the case $b_z=4\sqrt{c_k}$, where $k=2$ corresponds to strain distribution while $k=1$ to stress distribution. The dashed curve represents the classical solution.

$z=\pm\infty$. Both classical and gradient solutions may be obtained by a simple superposition of the solutions for a separate dislocation. In particular, for $y\to 0$ we have [60]

$$u_x|_{y\to 0}=\frac{b_x}{2}\operatorname{sign}(y)\left[\operatorname{sign}(x+d)\left(1-e^{-\frac{|x+d|}{\sqrt{c_2}}}\right)-\operatorname{sign}(x)\left(1-e^{-\frac{|x|}{\sqrt{c_2}}}\right)\right], \tag{24}$$

$$u_y|_{y\to 0}=\frac{b_x}{4\pi(1-\nu)}\left[-(1-2\nu)\left\{\ln\frac{|x|}{|x+d|}+K_0\left(\frac{|x|}{\sqrt{c_2}}\right)-K_0\left(\frac{|x+d|}{\sqrt{c_2}}\right)\right\}+\frac{2c_2}{x^2}-\frac{2c_2}{(x+d)^2}-K_2\left(\frac{|x|}{\sqrt{c_2}}\right)+K_2\left(\frac{|x+d|}{\sqrt{c_2}}\right)\right]. \tag{25}$$

The component $u_x(y\to 0)$ given by (24), coincides with the component $w_z(y\to 0)$ of a similar dipole of screw dislocations (see formula (21) and Figs. 1 and 2). From this analysis, we have concluded that in gradient elasticity a new characteristic distance appears, namely, the radius of strong short-range interaction between dislocations. It follows from the identity of expressions (21) and (24) that this conclusion is also valid for the case of edge dislocations [60].

The component $u_y(y\to 0)$ given by (25) is regular everywhere including the dislocation lines. In fact, for $x\to 0$ we have $K_0(|x|/\sqrt{c_2})|_{x\to 0}\to -\gamma-\ln\frac{|x|}{2\sqrt{c_2}}$ and $K_2(|x|/\sqrt{c_2})|_{x\to 0}\to 2\frac{c_2}{x^2}-\frac{1}{2}$, where γ=0.57721566… is Euler's constant. Thus,

$$u_y(x=0,y=0)=\frac{b_x}{4\pi(1-\nu)}\left[(1-2\nu)\times\left\{\gamma+\ln\frac{d}{2\sqrt{c_2}}+K_0\left(\frac{d}{\sqrt{c_2}}\right)\right\}+\frac{1}{2}-\frac{2c_2}{d^2}+K_2\left(\frac{d}{\sqrt{c_2}}\right)\right]. \tag{26}$$

It is seen from (26) that $u_y(0,0)$ increases with the dipole arm d and equals to zero when d=0. The dependence of $u_y(x,y=0)$ on d is presented in Fig. 8 which demonstrates the fact that the gradient solution is especially effective for describing the strong short-range interaction between dislocations.

The plots of Fig. 8c have been obtained numerically in [60] for a dislocation dipole with arm $d=100\sqrt{c_2}$ which may thus approximate the field of a separate dislocation. The gradient solution gives smaller displacements near the dislocation line ($-0.3\sqrt{c_2}\le x\le 0.3\sqrt{c_2}$) and larger ones outside of this region. With these plots, we have a possibility to compare the calculated value of the displacement $u_y(0,0)$ at the dislocation line with data from experimental observations and computer simulations. In considering u_y for a dislocation dipole with arm $d=100\sqrt{c_2}$, we have the estimate $u_y(0,0)\approx 2.3b_x/[4\pi(1-\nu)]$ which gives $\approx 0.26a$ for $b_x=a$ and ν=0.3. This value is in a good agreement with the results of direct observation of edge dislocations near an Nb/Al_2O_3 interface [67], as well as with the results of computer simulations for the core of an edge dislocation in α-Fe [68]. It is worth noting that this estimate can not be obtained within a Peierls-Nabarro dislocation model [1] because the latter imposes that the u_y displacement is identically zero.

Let us now consider the behavior of the elastic strain and stress components given by superpositions of formulae (10)–(11) with (14)–(15) near the dislocation line. The strain expessions (10) with (14) have been obtained in [60]. The stress expressions (11) with (15) reported in [61, 62], are represented in a closed form in contrast to the ones obtained in an integral form by Eringen [41] for the stress field of an edge dislocation within his version of non-local elastisity. The main feature of the solution given by (10)-(11) with (14)-(15) is the absence of any singularities in the strain and stress fields (previous models eliminated either the displace-

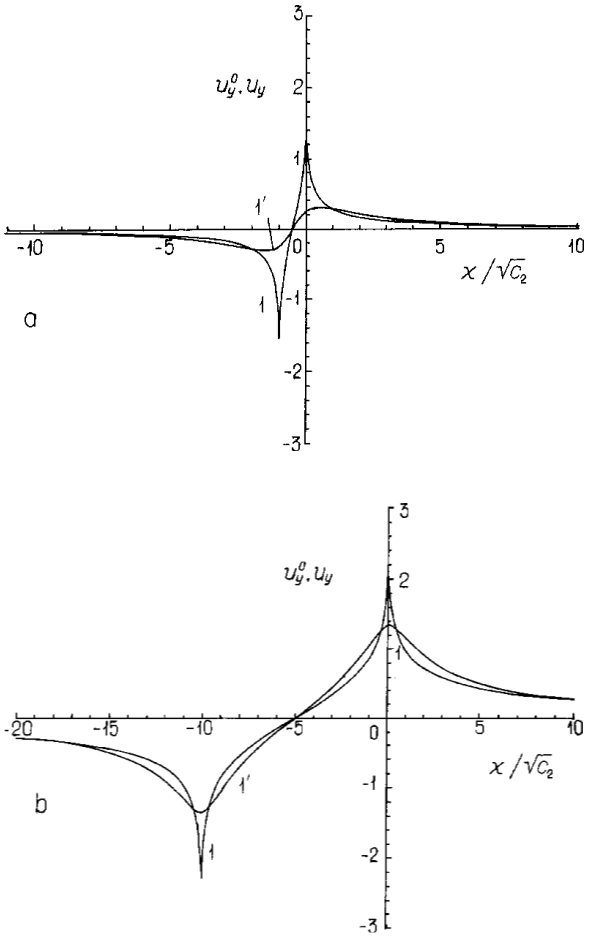

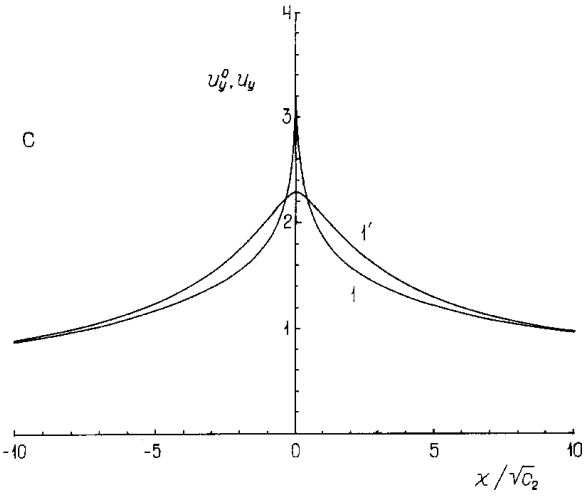

Fig. 8. The y-components of total displacement of a dipole of edge dislocations along the plane $y=0$ when the dipole arm d is equal to $1\sqrt{c_2}$ (a), $10\sqrt{c_2}$ (b) and $100\sqrt{c_2}$ (c); 1 – classical solution $u_y^0(x,y=0)$, 1' – gradient solution $u_y(x,y=0)$. The displacement values are given in units of $b_x/[4\pi(1-\nu)]$.

ment and strain singularity or the stress singularity but not both). One can note some interesting details in the behavior of the gradient solution [60].

From Fig. 9, one can conclude that the component $\varepsilon_{xx}(x=0)$ is smaller than $\varepsilon_{xx}^0(x=0)$ for $0\le|y|\le1.3\sqrt{c_2}$ and larger than $\varepsilon_{xx}^0(x=0)$ for $|y|\ge1.3\sqrt{c_2}$. It achieves a maximum value ≈0.3 (all strain values are given here in units of $b_x/[4\pi(1-\nu)\sqrt{c_2}]$) at $|y|\approx\sqrt{c_2}$ which gives ≈14% for an atomic lattice. The component $\varepsilon_{yy}(x=0)$ is smaller than $\varepsilon_{yy}^0(x=0)$ everywhere, it is equal to zero at $|y|\approx0.6\sqrt{c_2}$ and achieves two extrema values of opposite signs (on the same side of the dislocation line) which are equal to ≈0.01 (≈0.5%) at $\approx0.2\sqrt{c_2}$, and ≈0.06 (≈3%) at $\approx4\sqrt{c_2}$. It is interesting to note that $\varepsilon_{yy}(x=0)$ is significantly smaller than $\varepsilon_{xx}(x=0)$, in contrast to the classical solution where $\varepsilon_{yy}^0(x=0)\equiv\varepsilon_{xx}^0(x=0)$. The behavior of the dilatation $\varepsilon=\varepsilon_{xx}+\varepsilon_{yy}$ is similar to the behavior of the strain component ε_{xz} of a screw dislocation (see Section 3.1.2). The dilatation has maximum value of about 0.3 (≈14%) at $|y|\approx\sqrt{c_2}$, it is equal to zero at the dislocation line and practically coincides with the classical solution outside of the dislocation core ($|y|>4\sqrt{c_2}$). The shear component ε_{xy} is smaller than ε_{xy}^0 everywhere, it approaches zero at the dislocation line, achieves maximum values of about 0.25 (≈12%) at $|x|\approx1.5\sqrt{c_2}$ and practically coincides with ε_{xy}^0 far from the dislocation line ($|x|>10\sqrt{c_2}$).

A general (three-dimensional) view of the spatial distribution of elastic strains near the dislocation line [58] is provided in Fig. 10 which demonstrates all aforementioned features of gradient solution for the strain field.

Similar spatial distribution of stress components σ_{xx} and σ_{yy} near the dislocation line [61] are represented in Fig. 11. The distribution of shear stress component σ_{xy} is the same as that of shear strain component ε_{xy} (Fig. 10.c) with appropriate replacement of strain units of $b_x/[4\pi(1-\nu)\sqrt{c_2}]$ with stress units of $\mu b_x/[2\pi(1-\nu)\sqrt{c_1}]$ and coordinate units $(x,y)/\sqrt{c_2}$ with $(x,y)/\sqrt{c_1}$. Also, the distribution of hydrostatic stress component $\sigma=(\sigma_{xx}+\sigma_{yy}+\sigma_{zz})/3$ is the same as that of dilatation ε (Fig. 10.d) with similar replacement of units ($b_x/[4\pi(1-\nu)\sqrt{c_2}]$ with $\mu b_x(1+\nu)/[6\pi(1-\nu)(1-2\nu)\sqrt{c_1}]$, and $(x,y)/\sqrt{c_2}$ with $(x,y)/\sqrt{c_1}$). One can see that the gradient solutions for the stresses attain their extreme values ($|\sigma_{xx}|\approx0.45\mu$ and $|\sigma_{yy}|\approx|\sigma_{xy}|\approx0.27\mu$ for $b_x=a=4\sqrt{c_1}$ and $\nu=0.3$) at a distance $\approx a/4$ from the dislocation line. It is also seen that

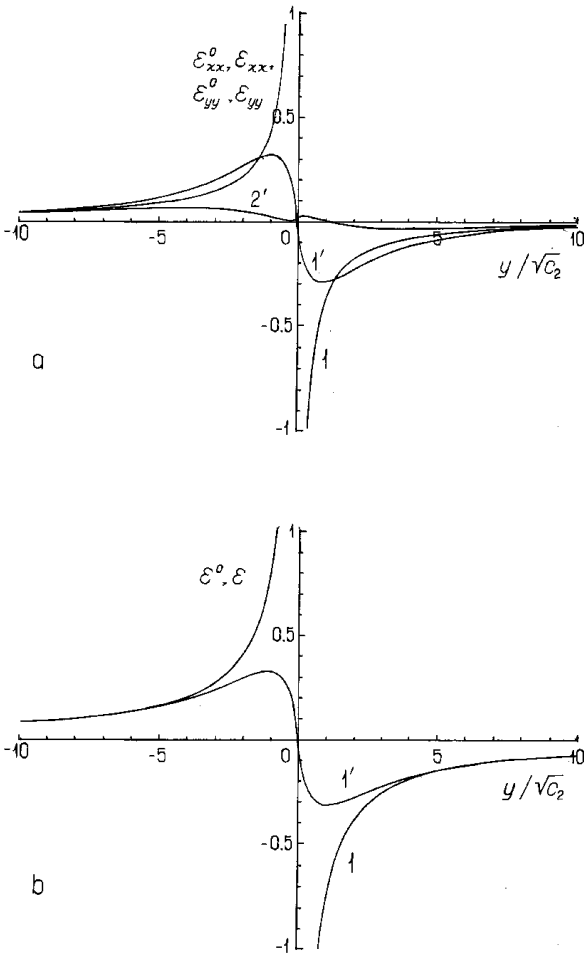

Fig. 9. The strain components (a) $\varepsilon^0_{xx}(x=0,y) \equiv \varepsilon^0_{yy}(x=0,y) - 1$, $\varepsilon_{xx}(x=0,y) - 1'$, $\varepsilon_{yy}(x=0,y) - 2'$; (b) $\varepsilon^0(x=0,y) - 1$, $\varepsilon(x=0,y) - 1'$; (c) $\varepsilon^0_{xy}(x,y=0) - 1$, $\varepsilon_{xy}(x,y=0) - 1'$ near the dislocation line. The strain values are given in units of $b_x/[4\pi(1-\nu)\sqrt{c_2}]$.

the gradient solutions coincide with the classical ones far away from the dislocation core ($r \geq r_0 \approx 4\sqrt{c_k}$) [60].

Thus, in considering the straight dislocations in a homogeneous elastic isotropic solid within the gradient theory of elasticity described by (5), one can summarize that new gradient solution gives non-singular expressions for dislocation displacement, strain and stress fields and elastic energies. It has been shown that for individual dislocations, the elastic strains and stresses are strictly equal to zero at the dislocation lines and achieve their extreme values of ≈(3÷14)% and ≈ (μ/4 ÷ μ/2), respectively, at a distance ≈a/4 from the dislocation line. Two characteristic distances appear naturally in this approach: $r_0 \approx 4\sqrt{c_2}$ which may be viewed as the radius of dislocation core and $d_0 \approx 10\sqrt{c_2}$ which may be viewed as the radius of strong short-range interaction between dislocations.

3.2. Straight dislocations near interfaces

A description of the elastic interaction of dislocations with interphase boundaries has been one of the key problems in the theory of defects, with applications to materials science and engineering and special attention to polycrystalline, multilayered and thin-film solid systems (e.g. [1, 11, 12, 69-73]). This description is traditionally based on solutions of appropriate boundary-value problems in the classical linear theory of elasticity. The corresponding solutions provide the elastic fields of dislocations far from both the interface and the dislocation line, thus being satisfactory for the cases when long-range elastic interactions are of interest. However, when short-range interactions are of interest, the classical solutions lead to unreasonable results. These concern the elastic singularity at the dislocation line, as well as the "image" force which acts on dislocations from the side of an interface which also becomes singular when the dislocation approaches the interface. Moreover, some components of the elastic stress field of a dislocation suffer jumps at the interface, a fact which may be acceptable from a macroscopic point of view but physically unrealistic from a nano- or microscopic point of view. To avoid the aforementioned three difficulties, the boundary-value problem of a straight dislocation near a flat interface has been reconsidered [64-66] within the theory of gradient elasticity described by (5).

3.2.1. A general solution

Consider a flat interface which separates two elastic isotropic media denoted by 1 (x>0) and 2 (x<0) with shear moduli μ_i, Poisson ratios ν_i, and gradient coefficients c_{1i} and c_{2i}, where i=1,2, respectively (Fig. 12). Let a straight dislocation having Burgers vector $\boldsymbol{b}=b_x\boldsymbol{e}_x+b_y\boldsymbol{e}_y+b_z\boldsymbol{e}_z$ goes through the point ($x=x'$,y=0) along the z-axis of a Carthesian coordinate system.

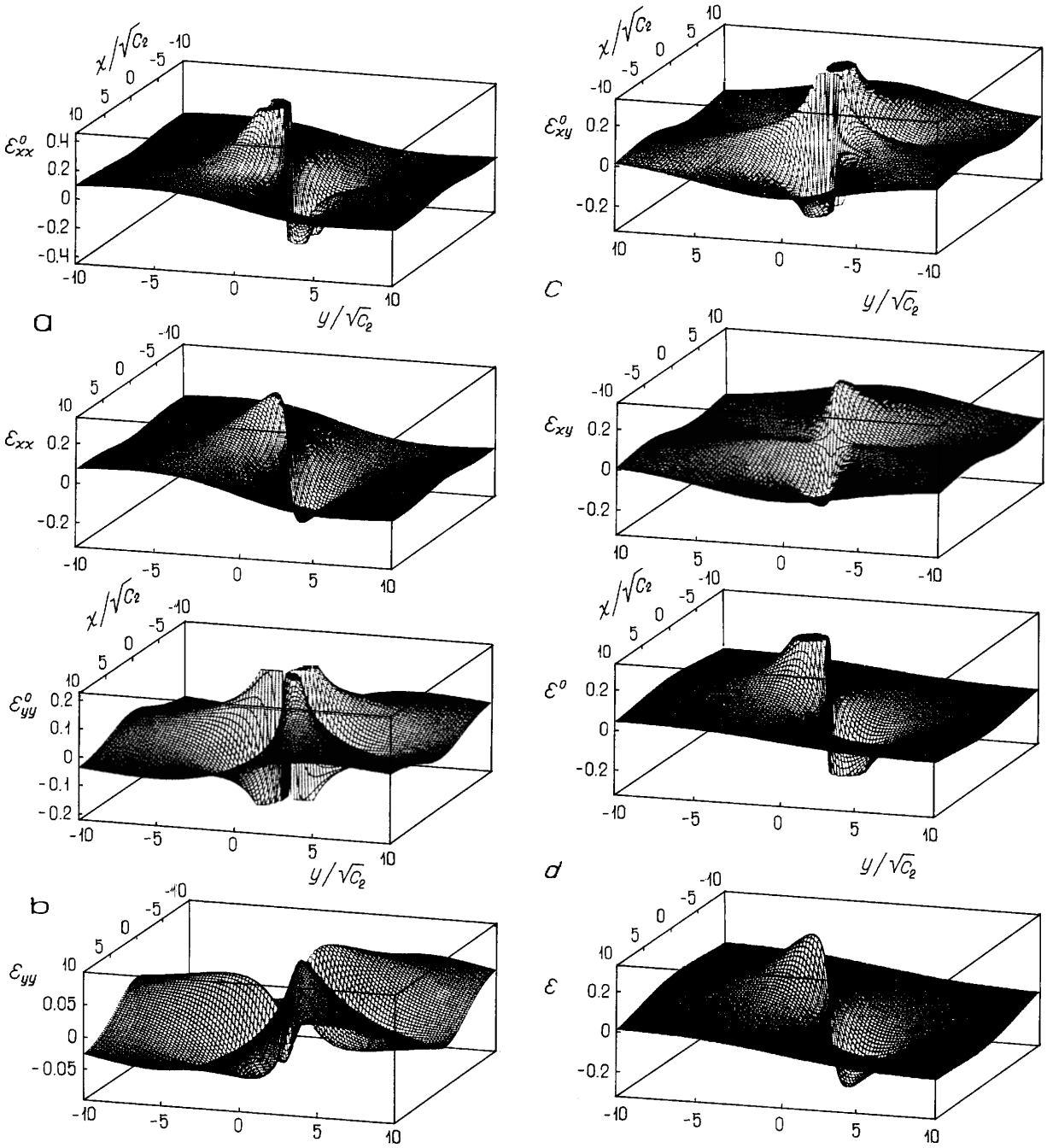

Fig. 10. The strain components ε_{xx} – (a), ε_{yy} – (b), ε_{xy} – (c), and ε – (d) near the line of an edge dislocation which goes through the point (0,0). The strain values are given in units of $b_x/[(4\pi(1-\nu)\sqrt{c_2}]$. The top figures give the classical singular solutions while the bottom ones give the gradient regular solutions.

Classical solution

In the framework of classical elasticity theory (where $c_{1i}=c_{2i}\equiv 0$), for $x'\geq 0$, the dislocation stress field is given [69] (in units of $\mu_1/[\pi(k_1+1)]$) in the medium 1 by

$$\sigma_{xx}^{0(1)} = b_x\left\{-\frac{2y}{r_-^2}-\frac{4yx_-^2}{r_-^4}+\frac{(A+B)y}{r_+^2}+\frac{4Ay(x'^2+x^2)}{r_+^4}+\frac{32\,Ayxx'x_+^2}{r_+^6}\right\}+b_y\left\{-\frac{2x_-}{r_-^2}+\frac{4x_-^3}{r_-^4}+\frac{(A+B)x-(3A-B)x'}{r_+^2}+\frac{4Ax_+(x'^2-6x'x-x^2)}{r_+^4}+\frac{32\,Axx'x_+^3}{r_+^6}\right\}, \tag{27}$$

$$\sigma_{yy}^{0(1)} = b_x\left\{-\frac{2y}{r_-^2}+\frac{4yx_-^2}{r_-^4}+\frac{(3A-B)y}{r_+^2}+\frac{4Ay(3x'^2+4x'x-x^2)}{r_+^4}-\frac{32\,Ayxx'x_+^2}{r_+^6}\right\}+b_y\left\{\frac{6x_-}{r_-^2}-\frac{4x_-^3}{r_-^4}\right.$$

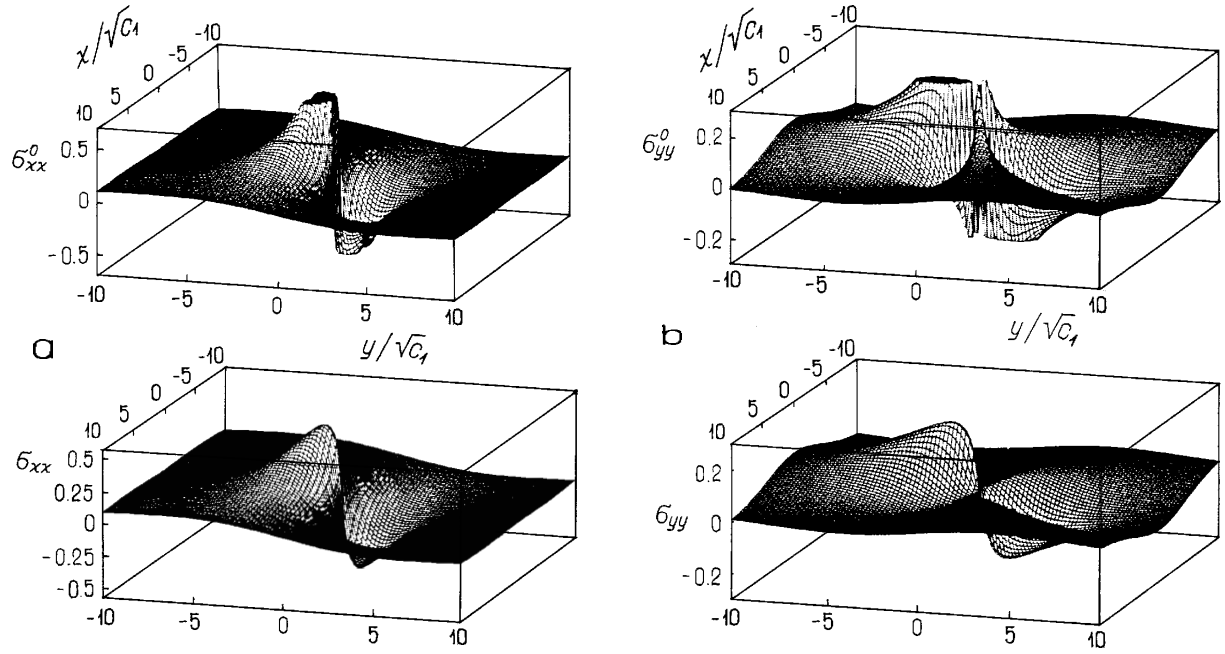

Fig. 11. The stress components σ^0_{xx}, σ_{xx} – (a) and σ^0_{yy}, σ_{yy} – (b) near the line of an edge dislocation which goes through the point (0,0). The stress values are given in units of $\mu b_x/[2\pi(1\text{-}\nu)\sqrt{c_1}]$. The top figures give the classical solutions σ^0_{ij} while the bottom ones give the gradient solution σ_{ij}.

$$-\frac{(5A+B)x+(9A+B)x'}{r_+^2}+\frac{4Ax_+(3x'^2+10x'x+x^2)}{r_+^4}$$
$$-\frac{32Axx'x_+^3}{r_+^6}\Bigg\}, \tag{28}$$

$$\sigma^{0(1)}_{xy}=b_x\left\{-\frac{2x_-}{r_-^2}+\frac{4x_-^3}{r_-^4}+\frac{(3A-B)x-(A+B)x'}{r_+^2}+\right.$$
$$\frac{4Ax_+(x'^2+6x'x-x^2)}{r_+^4}-\frac{32Axx'x_+^3}{r_+^6}\Bigg\}+b_y\left\{-\frac{2y}{r_-^2}+\right.$$
$$\frac{4yx_-^2}{r_-^4}+\frac{(A+B)y}{r_+^2}-\frac{4Ay(x'^2+4x'x+x^2)}{r_+^4}+ \tag{29}$$
$$\left.\frac{32Ayxx'x_+^2}{r_+^6}\right\},$$

$$\sigma^{0(1)}_{zz}=\nu_1(\sigma^{0(1)}_{xx}+\sigma^{0(1)}_{yy}), \tag{30}$$

$$\sigma^{0(1)}_{xz}=b_z\frac{k_1+1}{2}\left\{-\frac{y}{r_-^2}+\frac{\Gamma-1}{\Gamma+1}\frac{y}{r_+^2}\right\}, \tag{31}$$

$$\sigma^{0(1)}_{yz}=b_z\frac{k_1+1}{2}\left\{\frac{x_-}{r_-^2}+\frac{\Gamma-1}{\Gamma+1}\frac{x_+}{r_+^2}\right\}, \tag{32}$$

and in the medium 2 by

$$\sigma^{0(2)}_{xx}=b_x\left\{\frac{(A+B-2)y}{r_-^2}-\right.$$
$$\left.\frac{4yx_-[(1-B)x-(1-A)x']}{r_-^4}\right\}+$$
$$b_y\left\{\frac{(A+B-2)x+(B-3A+2)x'}{r_-^2}+\right. \tag{33}$$
$$\left.\frac{4x_-^2[(1-B)x-(1-A)x']}{r_-^4}\right\},$$

$$\sigma^{0(2)}_{yy}=b_x\left\{\frac{(3B-A-2)y}{r_-^2}+\right.$$
$$\left.\frac{4yx_-[(1-B)x-(1-A)x']}{r_-^4}\right\}+$$
$$b_y\left\{\frac{(6-5B-A)x+3(B+A-2)x'}{r_-^2}-\right. \tag{34}$$
$$\left.\frac{4x_-^2[(1-B)x-(1-A)x']}{r_-^4}\right\},$$

$$\sigma_{xy}^{0(2)} = b_x \left\{ \frac{(3B - A - 2)x + (2 - A - B)x'}{r_-^2} + \frac{4x_-[(1-B)x - (1-A)x']}{r_-^4} \right\} + b_y \left\{ \frac{(A + B - 2)y}{r_-^2} + \frac{4yx_-[(1-B)x - (1-A)x']}{r_-^4} \right\}, \quad (35)$$

$$\sigma_{zz}^{0(2)} = \nu_2(\sigma_{xx}^{0(2)} + \sigma_{yy}^{0(2)}), \quad (36)$$

$$\sigma_{xz}^{0(2)} = -b_z \frac{\Gamma(k_1+1)}{\Gamma+1} \frac{y}{r_-^2}, \quad (37)$$

$$\sigma_{yz}^{0(2)} = b_z \frac{\Gamma(k_1+1)}{\Gamma+1} \frac{x_-}{r_-^2}, \quad (38)$$

where $x_\pm = x \pm x'$, $r_\pm^2 = x_\pm^2 + y^2$, $A=(1-\Gamma)/(1+k_1\Gamma)$, $B=(k_2-k_1\Gamma)/(k_2+\Gamma)$, $\Gamma=\mu_2/\mu_1$, $k_i=3-4\nu_i$, i=1,2.

It is easily to see that the components σ_{xx}^0, σ_{xy}^0 and σ_{xz}^0 are continuous at the interface (x=0) while the components σ_{yy}^0, σ_{zz}^0 and σ_{yz}^0 suffer jumps $[\sigma_{kl}^0] = \sigma_{kl}^{0(1)} - \sigma_{kl}^{0(2)}$ there [64-66] which are (in units of $\mu_1/[\pi(1-\nu_1)]$)

$$\left[\sigma_{yy}^0\right]_{x=0} = \frac{(A-B)b_x y - (3A+B)b_y x'}{x'^2+y^2} + \frac{4A(b_x y + b_y x')x'^2}{(x'^2+y^2)^2}, \quad (39)$$

$$\left[\sigma_{zz}^0\right]_{x=0} = \frac{\nu_1[(A-1)b_x y - (3A+1)b_y x']}{x'^2+y^2} - \frac{\nu_2(B-1)(b_x y + b_y x')}{x'^2+y^2} + \frac{4\nu_1 A(b_x y + b_y x')x'^2 - 2\nu_2(A-1)b_y x'^3}{(x'^2+y^2)^2}, \quad (40)$$

$$\left[\sigma_{yz}^0\right]_{x=0} = b_z(1-\nu_1)\frac{\Gamma-1}{\Gamma+1}\frac{x'}{x'^2+y^2}. \quad (41)$$

Such jumps are expected from the macroscopic viewpoint of classical elasticity because these components do not give any contribution to the x-component of the elastic force which has to be in equilibrium at the interface. On the other hand, in considering the stressed state of an ideally welded interface from a nanoscopic point of view, the nature of this jump is not quite clear. In fact, the atomic layers on both sides of the interface interact elastically not only with atoms of their own material but also with atoms of the opposite material. Therefore, one has to assume the existence of a transitional zone of a few atomic layers where elastic interactions between atoms vary smoothly from stronger ones which are characteristic of one bulk material, to weaker ones which are characteristic of the other bulk material. It follows from this assumption, that stress jumps like (39)-(41) is only a consequence of the approximation of classical continuum models which often become insufficient for describing nanoscale phenomena. To demonstrate this fact, we note that the stress jumps in (39)-(41) tend to infinity in the xz-plane when the dislocation approaches the interface. It may thus be desirable for the interface stress jumps to be eliminated from the solution of this problem within any generalized theory of elasticity aiming to consider nanoscale phenomena.

Gradient solution

Let us now consider the corresponding dislocation fields within the theory of gradient elasticity given by (5). As proposed in [55] and described also in [61-63] (see Section 2.2), one can obtain the solution of (5) by solving separately Eqs. 7 and 8 for strain $\boldsymbol{\varepsilon}$ and stress $\boldsymbol{\sigma}$ fields, respectively, in terms of the strain $\boldsymbol{\varepsilon}^0$ and stress $\boldsymbol{\sigma}^0$ fields of the classical elasticity theory for the same boundary-value problem. Here we consider only the solution of Eq. 8 for stress field because it is especially important for applications.

Eq. 8 can be solved [61-66] by using the Fourier transform method. Rewrite the stress equation in the form

$$(1 - c_{l_i}\nabla^2)\boldsymbol{\sigma}^{(i)} = \boldsymbol{\sigma}^{0(i)}, \quad (42)$$

where $\boldsymbol{\sigma}^{0(i)}$ are given by (27)-(38). Below we will omit for simplicity the first index "1" at the gradient coefficient c_{1_i} in which case c_1 will refer to the material 1 and c_2 to the material 2. Basing on above notes to the classical solution as well as on conclusions of Ru and Aifantis [49, 55], we use [64-66] the classical boundary conditions

$$\left[\sigma_{xl}\right]_{x=0} = 0, \quad l = x, y, z, \quad (43)$$

and nine extra boundary conditions

$$\left[\sigma_{yy}\right]_{x=0}=\left[\sigma_{zz}\right]_{x=0}=\left[\sigma_{yz}\right]_{x=0}=\left[\frac{\partial\sigma_{kl}}{\partial x}\right]_{x=0}=0,\qquad k,l=x,y,z, \tag{44}$$

Last equation in (44) provide for smooth transitions of stress components through the interface.

Omitting intermediate calculations, we give here only the final results. The gradient solution [64-66] reads $\sigma_{kl}^{(i)}=\sigma_{kl}^{0(i)}+\sigma_{kl}^{gr(i)}$, where $\sigma_{kl}^{0(i)}$ are given by (27)-(38) and $\sigma_{kl}^{gr(i)}$ are (in units of $\mu_1/[\pi(k_1+1)]$), for medium 1

$$\begin{aligned}\sigma_{xx}^{gr(1)}&=4b_x\left\{y^3\Phi_1(r_-)+y(3x_-^2-y^2)\Phi_2(r_-)-\frac{2Ac_1y}{r_+^6}\left[3x_+^2-y^2+24x'x_+\frac{x_+^2-y^2}{r_+^2}\right]\right.\\&\left.+\int_0^\infty\frac{s^2\sin(sy)}{\lambda_1+\lambda_2}e^{-x\lambda_1}\left[c_1s\frac{\lambda_2-\lambda_1}{\lambda_1}e^{-x'\lambda_1}+\{Ac_1(\lambda_2+s)(1+2x's)-c'(\lambda_2-s)\}e^{-x's}\right]ds\right\}\\&+4b_y\left\{-x_-y^2\Phi_1(r_-)-x_-(x_-^2-3y^2)\Phi_2(r_-)+\frac{2Ac_1}{r_+^6}\left[x_+(x_+^2-3y^2)-6x'\frac{x_+^4-6x_+^2y^2+y^4}{r_+^2}\right]\right.\\&\left.+\int_0^\infty\frac{s^2\cos(sy)}{\lambda_1+\lambda_2}e^{-x\lambda_1}\left[c_1(\lambda_2-\lambda_1)e^{-x'\lambda_1}-\{Ac_1(\lambda_2+s)(1-2x's)+c'(\lambda_2-s)\}e^{-x's}\right]ds\right\},\end{aligned} \tag{45}$$

$$\begin{aligned}\sigma_{yy}^{gr(1)}&=4b_x\left\{x_-^2y\Phi_1(r_-)-y(3x_-^2-y^2)\Phi_2(r_-)+\frac{2Ac_1y}{r_+^6}\left[3x_+^2-y^2+24x'x_+\frac{x_+^2-y^2}{r_+^2}\right]\right.\\&\left.-\int_0^\infty\frac{\lambda_1^2\sin(sy)}{\lambda_1+\lambda_2}e^{-x\lambda_1}\left[c_1s\frac{\lambda_2-\lambda_1}{\lambda_1}e^{-x'\lambda_1}+\{Ac_1(\lambda_2+s)(1+2x's)-c''(\lambda_2-s)\}e^{-x's}\right]ds\right\}\\&+4b_y\left\{-x_-^3\Phi_1(r_-)+x_-(x_-^2-3y^2)\Phi_2(r_-)-\frac{2Ac_1}{r_+^6}\left[x_+(x_+^2-3y^2)-6x'\frac{x_+^4-6x_+^2y^2+y^4}{r_+^2}\right]\right.\\&\left.-\int_0^\infty\frac{\lambda_1^2\cos(sy)}{\lambda_1+\lambda_2}e^{-x\lambda_1}\left[c_1(\lambda_2-\lambda_1)e^{-x'\lambda_1}-\{Ac_1(\lambda_2+s)(1-2x's)+(B+c's^2)(\lambda_2-s)/\lambda_1^2\}e^{-x's}\right]ds\right\},\end{aligned} \tag{46}$$

$$\begin{aligned}\sigma_{xy}^{gr(1)}&=4b_x\left\{-x_-y^2\Phi_1(r_-)-x_-(x_-^2-3y^2)\Phi_2(r_-)+\frac{2Ac_1}{r_+^6}\left[x_+(x_+^2-3y^2)+6x'\frac{x_+^4-6x_+^2y^2+y^4}{r_+^2}\right]\right.\\&\left.+\int_0^\infty\frac{s\cos(sy)}{\lambda_1+\lambda_2}e^{-x\lambda_1}\left[c_1s(\lambda_2-\lambda_1)e^{-x'\lambda_1}+\{B-Ac_1(\lambda_1^2+\lambda_2s)(1+2x's)-c's(\lambda_2-s)\}e^{-x's}\right]ds\right\}\\&+4b_y\left\{x_-^2y\Phi_1(r_-)-y(3x_-^2-y^2)\Phi_2(r_-)+\frac{2Ac_1y}{r_+^6}\left[3x_+^2-y^2-24x'x_+\frac{x_+^2-y^2}{r_+^2}\right]\right.\\&\left.-\int_0^\infty\frac{s\sin(sy)}{\lambda_1+\lambda_2}e^{-x\lambda_1}\left[c_1\lambda_1(\lambda_2-\lambda_1)e^{-x'\lambda_1}+\{B+Ac_1(\lambda_1^2+\lambda_2s)(1-2x's)-c's(\lambda_2-s)\}e^{-x's}\right]ds\right\},\end{aligned} \tag{47}$$

$$\begin{aligned}\sigma_{zz}^{gr(1)}&=4\nu_1\left\{(b_xy-b_yx_-)r_-^2\Phi_1(r_-)-b_x\int_0^\infty\frac{\sin(sy)}{\lambda_1+\lambda_2}e^{-x\lambda_1}\left[s\frac{\lambda_2-\lambda_1}{\lambda_1}e^{-x'\lambda_1}\right.\right.\\&\left.\left.+\{A(\lambda_2+s)(1+2x's)-[(B-1)\nu_2/\nu_1+1](\lambda_2-s)\}e^{-x's}\right]ds\right.\\&\left.-b_y\int_0^\infty\frac{\cos(sy)}{\lambda_1+\lambda_2}e^{-x\lambda_1}\left[(\lambda_2-\lambda_1)e^{-x'\lambda_1}-\{A[s+\lambda_2(1-2x's)]+[(B-1)\nu_2/\nu_1+1](\lambda_2-s)\}e^{-x's}\right]ds,\right.\end{aligned} \tag{48}$$

$$\sigma_{xz}^{gr(1)} = b_z \frac{k_1+1}{2}\left\{ y r_-^2 \Phi_1(r_-) + \int_0^\infty \frac{s\sin(sy)}{\lambda_1+\lambda_2} e^{-x\lambda_1}\left(\frac{\lambda_1-\lambda_2}{\lambda_1} e^{-x'\lambda_1} + 2\frac{\Gamma-1}{\Gamma+1} e^{-x's} \right) ds \right\}, \tag{49}$$

$$\sigma_{yz}^{gr(1)} = b_z \frac{k_1+1}{2}\left\{ -x_- r_-^2 \Phi_1(r_-) - \int_0^\infty \frac{\lambda_1\cos(sy)}{\lambda_1+\lambda_2} e^{-x\lambda_1}\left(\frac{\lambda_1-\lambda_2}{\lambda_1} e^{-x'\lambda_1} + 2\frac{\Gamma-1}{\Gamma+1} e^{-x's} \right) ds \right\}, \tag{50}$$

and for medium 2

$$\begin{aligned}
\sigma_{xx}^{gr(2)} &= 8(B-1)c_2\{-b_x y(3x_-^2 - y^2) + b_y x_-(x_-^2 - 3y^2)\}/r_-^6 \\
&-4b_x \int_0^\infty \frac{s^2\sin(sy)}{\lambda_1+\lambda_2} e^{x\lambda_2}\left[2c_1 s e^{-x'\lambda_1} + \{Ac_1(\lambda_1 - s)(1+2x's) - c'(\lambda_1+s)\} e^{-x's} \right] ds \\
&-4b_y \int_0^\infty \frac{s^2\cos(sy)}{\lambda_1+\lambda_2} e^{x\lambda_2}\left[2c_1\lambda_1 e^{-x'\lambda_1} - \{Ac_1(\lambda_1 - s)(1-2x's) + c'(\lambda_1+s)\} e^{-x's} \right] ds,
\end{aligned} \tag{51}$$

$$\begin{aligned}
\sigma_{yy}^{gr(2)} &= 8(B-1)c_2\{b_x y(3x_-^2 - y^2) - b_y x_-(x_-^2 - 3y^2)\}/r_-^6 \\
&+4b_x \int_0^\infty \frac{\lambda_1^2\sin(sy)}{\lambda_1+\lambda_2} e^{x\lambda_2}\left[2c_1 s e^{-x'\lambda_1} + \{Ac_1(\lambda_1 - s)(1+2x's) - c''(\lambda_1+s)\} e^{-x's} \right] ds \\
&+4b_y \int_0^\infty \frac{\lambda_1^2\cos(sy)}{\lambda_1+\lambda_2} e^{x\lambda_2}\left[2c_1\lambda_1 e^{-x'\lambda_1} - \{Ac_1(\lambda_1 - s)(1-2x's) + (B+c's^2)(\lambda_1+s)/\lambda_1^2\} e^{-x's} \right] ds,
\end{aligned} \tag{52}$$

$$\begin{aligned}
\sigma_{xy}^{gr(2)} &= 8(B-1)c_2\{b_x x_-(x_-^2 - 3y^2) + b_y y(3x_-^2 - y^2)\}/r_-^6 \\
&+4b_x \int_0^\infty \frac{s\cos(sy)}{\lambda_1+\lambda_2} e^{x\lambda_2}\left[-2c_1\lambda_1 s e^{-x'\lambda_1} + \{B - Ac_1\lambda_1(\lambda_1 - s)(1+2x's) + c's(\lambda_1+s)\} e^{-x's} \right] ds \\
&+4b_y \int_0^\infty \frac{s\sin(sy)}{\lambda_1+\lambda_2} e^{x\lambda_2}\left[2c_1\lambda_1^2 e^{-x'\lambda_1} - \{B + Ac_1\lambda_1(\lambda_1 - s)(1-2x's) + c'(\lambda_1+s)\} e^{-x's} \right] ds,
\end{aligned} \tag{53}$$

$$\begin{aligned}
\sigma_{zz}^{gr(2)} &= 4b_x\nu_1 \int_0^\infty \frac{\sin(sy)}{\lambda_1+\lambda_2} e^{x\lambda_2}\left[2s e^{-x'\lambda_1} + \{A(\lambda_1 - s)(1+2x's) - [(B-1)\nu_2/\nu_1 + 1](\lambda_1+s)\} e^{-x's} \right] ds \\
&+4b_y\nu_1 \int_0^\infty \frac{\cos(sy)}{\lambda_1+\lambda_2} e^{x\lambda_2}\left[2\lambda_1 e^{-x'\lambda_1} + \{A[s - \lambda_1(1-2x's)] - [(B-1)\nu_2/\nu_1 + 1](\lambda_1+s)\} e^{-x's} \right] ds,
\end{aligned} \tag{54}$$

$$\sigma_{xz}^{gr(2)} = b_z(k_1+1) \int_0^{+\infty} \frac{s\sin(sy)}{\lambda_1+\lambda_2} e^{x\lambda_2}\left(e^{-x'\lambda_1} + \frac{\Gamma-1}{\Gamma+1} e^{-x's} \right) ds, \tag{55}$$

$$\sigma_{yz}^{gr(2)} = b_z(k_1+1) \int_0^{+\infty} \frac{\lambda_2\cos(sy)}{\lambda_1+\lambda_2} e^{x\lambda_2}\left(e^{-x'\lambda_1} + \frac{\Gamma-1}{\Gamma+1} e^{-x's} \right) ds. \tag{56}$$

where $\Phi_1 = K_1(r/\sqrt{c_1})/(\sqrt{c_1}r^3)$, $\Phi_2 = [2c_1/r^2 - K_2(r/\sqrt{c_1})]/r^4$, $c' = c_1 + c_2(B\text{-}1)$, $c'' = c_1 + c_2(B\text{-}1)\lambda_2^2/\lambda_1^2$, and $\lambda_i = \sqrt{1/c_i + s^2}$, i=1,2.

The gradient stress components $\sigma_{kl}^{(i)}$ given by the superposition of the classical ones (27)-(38) and gradient extra terms (45)-(56), are continuous at the interface (x=0). When $\mu_1=\mu_2=\mu$, $\nu_1=\nu_2=\nu$, and $c_1 = c_2 = c$ (the case of a

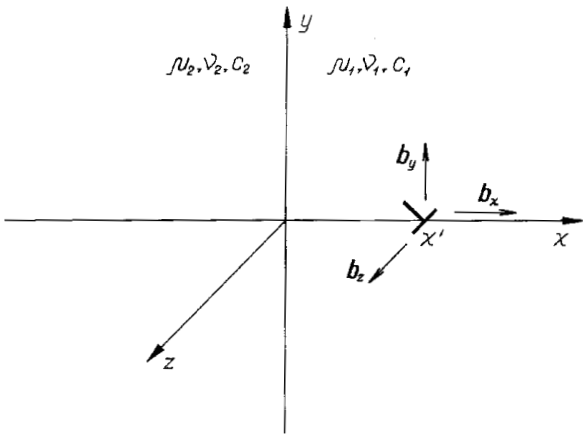

Fig. 12. A straight dislocation near a flat interface.

homogeneous medium), they are transformed into the superposition of (11) and (15). When $c_1 = c_2 \to 0$ (the limiting transition to the classical elasticity), the gradient extra terms (45)-(56) disappear. It is worth noting, that (45)-(56) contain specific terms caused only by a difference between the gradient coefficients c_1 and c_2 (see, for example, first subintegral terms).

Below, we consider separately the cases of screw and edge dislocations for the following three types of interfaces: a "purely elastic" interface ($\mu_1 \neq \mu_2$, $\nu_1 \neq \nu_2$, $c_1 = c_2 = c$), a "purely gradient" interface ($\mu_1 = \mu_2$, $\nu_1 = \nu_2$, $c_1 \neq c_2$), as well as a general "mixed gradient elastic" interface ($\mu_1 \neq \mu_2$, $\nu_1 \neq \nu_2$, $c_1 \neq c_2$).

3.2.2. Screw dislocations

For screw dislocations, the general solution is given [64, 65] by the superpositon of the classical expressions (31), (32), (37) and (38), and gradient extra terms (49), (50), (55) and (56).

Purely elastic interface ($\mu_1 \neq \mu_2$, $\nu_1 \neq \nu_2$, $c_1 = c_2 = c$)

In this case, the gradient solution (in units of $\mu_1 b_z/2\pi$) is [64, 65]

$$\sigma_{xz}^{(1,2)} = \sigma_{xz}^{0(1,2)} + \frac{y}{\sqrt{c}\, r_-} K_1\left(\frac{r_-}{\sqrt{c}}\right) + \frac{\Gamma - 1}{\Gamma + 1} \int_0^{+\infty} \frac{s}{\lambda} \sin(sy) e^{-|x|\lambda - x's} ds, \tag{57}$$

$$\sigma_{yz}^{(1,2)} = \sigma_{yz}^{0(1,2)} - \frac{x - x'}{\sqrt{c}\, r_-} K_1\left(\frac{r_-}{\sqrt{c}}\right) - \frac{\Gamma - 1}{\Gamma + 1} \operatorname{sign}(x) \int_0^{+\infty} \cos(sy) e^{-|x|\lambda - x's} ds, \tag{58}$$

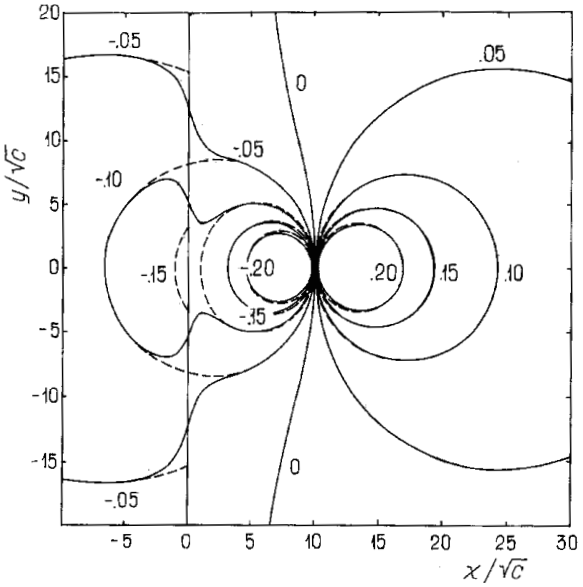

Fig. 13. Stress field σ_{yz} map for a screw dislocation located at the point $(10,0)$ near a flat interface (at $x=0$) separating two elastic media with $\mu_2 = 2\mu_1$ and $c_1 = c_2 = c$. The stresses are given in units of $\mu_1 b_z / (2\pi\sqrt{c})$. The dashed contours represent the classical solution σ_{yz}^0.

where $\sigma_{iz}^{0(1,2)}$ are determined by (31), (32), (37) and (38), and $\lambda = \sqrt{1/c + s^2}$. Both components are continuous at the interface, in contrast to the classical solution where σ_{yz}^0 suffers a jump given by (41). Figs. 13 and 14 illustrate this difference. It is seen that the magnitude of the jump increases as the dislocation approaches the interface. Also, the gradient solution is finite at the dislocation line, while the classical one is singular there (Fig. 14). It is seen that the classical and gradient solutions coincide far ($r > 5\sqrt{c}$) from the interface or the dislocation line, while they are quite different at nanoscopic distances from them ($r < 5\sqrt{c}$).

When the dislocation lies directly at the interface ($x'=0$), the integrals in (57)-(58) can be calculated in a closed form giving (in units of $\mu_1\mu_2 b_z/[\pi(\mu_1+\mu_2)]$)

$$\sigma_{xz} = -\frac{y}{r^2} + \frac{y}{\sqrt{c}\, r} K_1\left(\frac{r}{\sqrt{c}}\right), \qquad \sigma_{yz} = \frac{x}{r^2} + \frac{x}{\sqrt{c}\, r} K_1\left(\frac{r}{\sqrt{c}}\right), \tag{59}$$

where $r^2 = x^2 + y^2$. It is worth noting that the gradient solutions given by (59) for such an interface dislocation differ only by a factor $2\mu_2/(\mu_1+\mu_2)$ from those given by the corresponding components in the superposition of (11) and (15) for a screw dislocation in a single-phase infinite medium as is the case in the classical theory of elasticity.

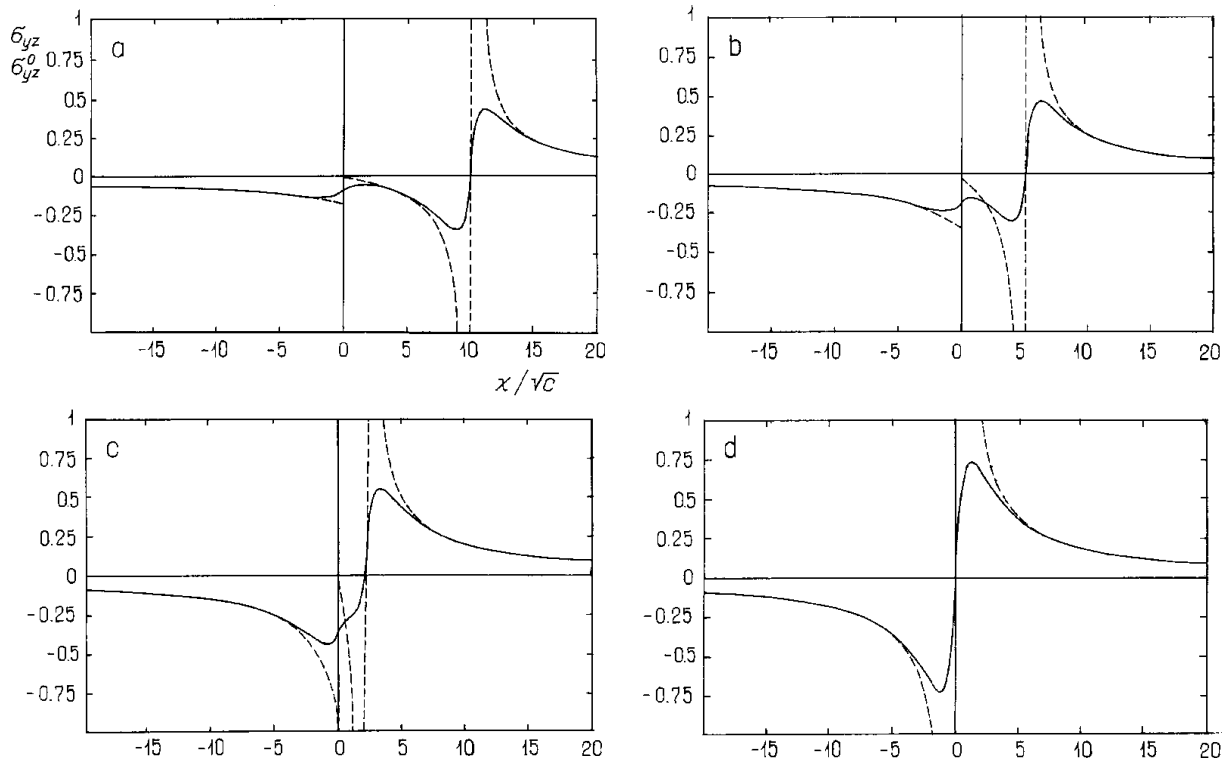

Fig. 14. The stress component $\sigma_{yz}(x,y=0)$ near the line of a screw dislocation located at a distance $x'/\sqrt{c} = 10$ (a), 5 (b), 2 (c) and 0 (d) from the interface (at $x=0$) of two elastic media with $\mu_2=10\mu_1$ and $c_1=c_2=c$. The stress values are given in units of $\mu_1 b_z / (2\pi\sqrt{c})$. The dashed curves represent the classical solution σ^0_{yz}.

Let us consider now the "image" force F_x^{el} which acts on the dislocation unit length due to the interface (Fig. 12). The gradient solution (in units of $\mu_1 b_z^2/2\pi$) reads [64, 65]

$$F_x^{el}(x') = b_z\sigma_{yz}^{(1)}(x=x',\ y=0) = \frac{\Gamma-1}{\Gamma+1}\left\{\frac{1}{2x'} - \int_0^{+\infty} e^{-x'(\lambda+s)}ds\right\}, \qquad (60)$$

where the first term in the brackets is the classical singular solution and the second one is the extra gradient term. The numerical evaluation of (60) is presented in Fig. 15 where also a similar solution for $x'<0$ is plotted. It is seen that the classical singularity is eliminated from the gradient solutions which attain maximum values at a distance $\approx\sqrt{c}$ from the interface and tend to zero at the interface.

This result is especially instructive for the case of a free surface when $\Gamma=0$ (see the negative-valued curves in Fig. 15). In fact, there is no image force when the dislocation lies at the free surface, the force emerges and increases when the dislocation begins to penetrate into the material (the estimated dislocation core radius is $\approx 4\sqrt{c}$ [59]), achieves a maximum value and decreases when the dislocation moves inside the material. The last stage is also well described by the classical solution (Fig. 15) which, however, can not describe at all the abovementioned preceding stages. Within the gradient theory of (5), one can estimate a maximum shear stress $\tau_{max}=|F_x^{el}|_{max}/b_z$ which the screw dislocation has to overcome for penetrating into the material. From Fig. 15, it is estimated that $\tau_{max}\approx\mu/2\pi$, i.e. the value of theoretical shear strength [1]. For the case of two bonded solids, the result of zero value at the interface (i.e., the appearance of an unstable equilibrium position there) is not as clear.

Purely gradient interface ($\mu_1=\mu_2=\mu$, $\nu_1=\nu_2=\nu$, $c_1\neq c_2$)

In this case, the corresponding gradient solution is given by the superposition of (31), (32), (37) and (38) with (49), (50), (55) and (56), respectively, with $\Gamma=1$. Here we focus only on the appropriate "image" force F_x^{gr} which acts upon the dislocation due to the difference in the gradient moduli c_1 and c_2. This force is given (in units of $\mu_1 b_z^2/2\pi$) by [64, 65]

$$F_x^{gr}(x') = b_z\sigma_{yz}^{(1)}(x=x',\ y=0) = -\int_0^{+\infty}\frac{\lambda_1-\lambda_2}{\lambda_1+\lambda_2}e^{-2x'\lambda_1}ds. \qquad (61)$$

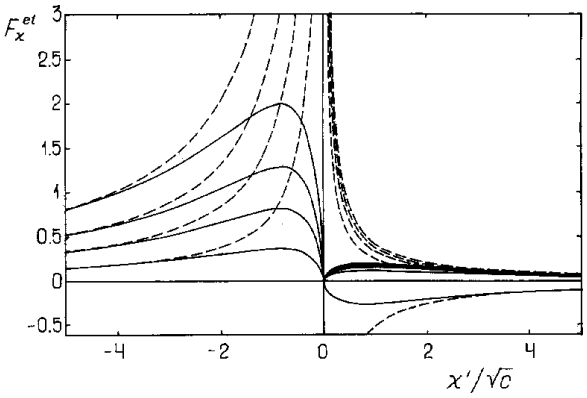

Fig. 15. The "image" force F_x^{el} which acts upon the dislocation unit length due to the interface (at $x=0$) of two elastic media with $c_1=c_2=c$ and $\mu_2/\mu_1=10$, 7, 5, 3 and 0 (from top to bottom), as a function of the dislocation position $x'/\sqrt{c}$. The force values are given in units of $\mu_1 b_z^2/(2\pi\sqrt{c})$. The dashed curves represent the classical solution.

When $c_1>c_2$, i.e. $\lambda_1<\lambda_2$, the integral in (61) is negative and the force F_x^{gr} is positive. This means that the dislocation is pushed away from the interface into the bulk of material 1 which has the larger gradient coefficient. This is in agreement with the gradient solution for the strain energy of a screw dislocation [58, 61] $W=\mu b_z^2/(4\pi)\{\gamma+\ln(R/2\sqrt{c_1})\}$ (see also (16) with $b_x=0$); indeed, the larger c_1 is, the smaller W is. Plots for $F_x^{gr}(x')$ are presented in Fig. 16 from which one can conclude that this force has a short-range character and acts just near the interface. At the interface, it attains a maximum value which depends strongly on the ratio c_2/c_1 (Fig. 16).

General mixed gradient elastic interface ($\mu_1\neq\mu_2$, $\nu_1\neq\nu_2$, $c_1\neq c_2$)

In this case, the gradient solution is given by the superposition of (31), (32), (37) and (38) with (49), (50), (55) and (56), respectively, and the "image" force F_x (in units of $\mu_1 b_z^2/2\pi$) is [64, 65]

$$F_x(x') = \frac{\Gamma-1}{\Gamma+1}\frac{1}{2x'} - \int_0^{+\infty}\frac{\lambda_1}{\lambda_1+\lambda_2}\times \left\{\frac{\lambda_1-\lambda_2}{\lambda_1}e^{-2x'\lambda_1} + 2\frac{\Gamma-1}{\Gamma+1}e^{-x'(\lambda_1+s)}\right\}ds. \quad (62)$$

It is worth noting that F_x is not a simple superposition of F_x^{el} and F_x^{gr} given by (60) and (61), respectively. However, it manifests their characteristic features (Fig. 17). Similar to F_x^{el}, the force in (62) is a nonsingular long-range force which coincides with the classical solution far ($|x'|>5\sqrt{c_1}$) from the interface. Similar to F_x^{gr}, it attains non-zero values at the interface which depend on both ratios μ_2/μ_1 and c_2/c_1. In fact, the sign and qualitative behavior of F_x near the interface is entirely determined by c_2/c_1. For example, if $\mu_2>\mu_1$, there are three different types of behavior of F_x (Fig. 17). When $c_2<c_1$, $F_x>0$ everywhere and attains maximum values near or at the interface. When $c_2=c_1$, $F_x\equiv F_x^{el}$ and becomes equal to zero at the interface (see above). When $c_2>c_1$, $F_x>0$ except at a small region around the interface. The size of this region which depends on c_2/c_1 is about $\sqrt{c_1}$, and $F_x<0$ inside this region attaining its minimum value at the interface. When $c_2<c_1$, the dislocation is pushed from material 2 into material 1 and has no equilibrium position. When $c_2=c_1$, it does the same but it has an unstable equilibrium position at the interface. When $c_2>c_1$, a dislocation being in material 2, is attracted to the interface and is locked at a stable equilibrium position $x'\approx-(0.2–0.8)\sqrt{c_1}$ near that interface, while a dislocation located in material 1, has an unstable equilibrium position $x'\approx(0.4\text{-}0.7)\sqrt{c_1}$ near the interface; being attracted to it within a small region $x'<(0.4–0.7)\sqrt{c_1}$ and pushed away from it otherwise.

3.2.3. Edge dislocations

For edge dislocations, the general solution is given [66] by the superpositon of the classical expressions (27)-(30) and (33)-(36), and gradient extra terms (45)-(48) and (51)-(54).

Purely elastic interface ($\mu_1\neq\mu_2$, $\nu_1\neq\nu_2$, $c_1=c_2=c$)

In this case, we consider the effects caused only by the difference in the elastic constants of the bonded media. Two main advantages of the gradient solution may be pointed out in this connection. First, there are no singularities in the stress components $\sigma_{kl}^{(i)}$ at the dislocation line. Second, there are no jumps like those given by (39)-(40) in $\sigma_{yy}^{(i)}$ and $\sigma_{zz}^{(i)}$ at the interface. This allows one to consider nanoscale short-range elastic interactions between dislocations and interfaces, in contrast to the classical singular solution (27)-(30) and (33)-(36), where the components $\sigma_{yy}^{0(i)}$ and $\sigma_{zz}^{0(i)}$ suffer jump discontinuities at the interface. This is illustrated in Fig. 18 for the component $\sigma_{yy}^{(i)}(x,0)$ of a dislocation with Burgers vector b_y. It is seen that classical and gradient solutions coincide far ($r>10\sqrt{c}$) from the interface or the dislocation line, while near them (within nanoscopic distances $r<10\sqrt{c}$) they are quite different.

Let us consider now the "image" force F_x^{el} which acts upon the dislocation unit length by the interface (Fig. 12). For a dislocation with Burgers vector b_x, the gradient solution $F_x^{el}(x')=b_x\sigma_{xy}^{(1)}(x=x',0)$ reads (in units of $\mu_1 b_x^2/[\pi(k_1+1)]$) [66]

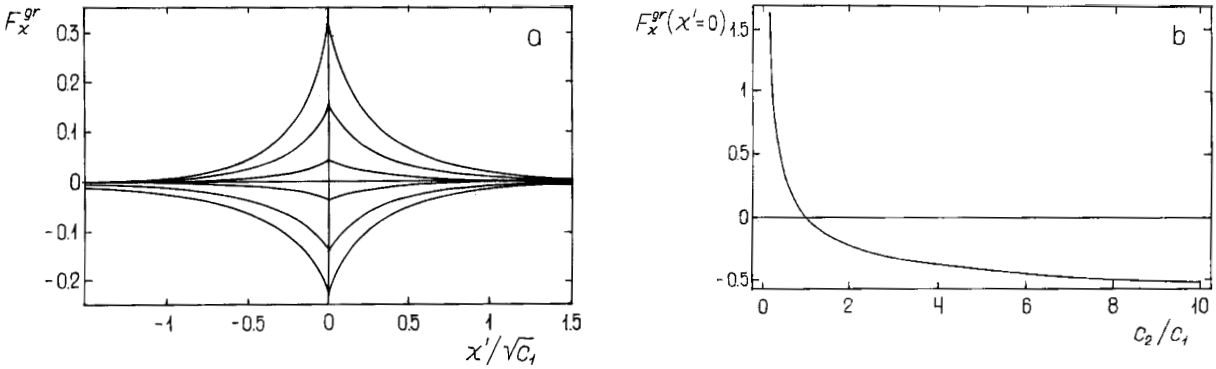

Fig. 16. The "image" force F_x^{gr} which acts upon the dislocation unit length due to the interface (at x=0) of two elastic media with $\mu_2=\mu_1$ and c_2/c_1=0.5, 0.7, 0.9, 1.1, 1.5 and 2 (from top to bottom), as a function of the dislocation position $x'/\sqrt{c_1}$ (a). The values of the image force at the interface $F_x^{gr}(x'=0)$ as a function of the ratio c_2/c_1 (b). The force values are given in units of $\mu_1 b_z^2/(2\pi\sqrt{c_1})$.

$$F_x^{el}(x') = -\frac{A+B}{2x'} + \frac{4Ac}{x'^3} + 2c\int_0^{+\infty} s[B(\lambda-s) - A(\lambda+s)(1+2x's)]e^{-x'(\lambda+s)}ds, \quad (63)$$

where $\lambda = \sqrt{1/c + s^2}$. The first term in this expression is the classical singular solution, while the remaining two are extra gradient terms. The numerical evaluation of (63) is presented in Fig. 19 where also a similar solution for $x'<0$ is plotted. It is seen that the classical singularity is eliminated from the gradient solution which attains maximum values at a distance $\approx\sqrt{c}$ from the interface and has no jumps at the interface.

In the case of a free surface when $\mu_2=\nu_2=0$ (see the negative-valued curves of Fig. 19), the situation is just like with a screw dislocation (see Section 3.2.2). So, there is no image force when the dislocation lies at the free surface. The force appears and increases when the dislocation begins to penetrate into the material, achieves a maximum value and decreases when the dislocation moves inside the material. Again, the last stage (for $x'>5\sqrt{c}$) is also well described by the classical solution (Fig. 19). Within the gradient theory (5), one can estimate a maximum shear stress $\tau_{max}=|F_x^{el}|_{max}/b_x$ which the edge dislocation has to overcome in order to penetrate inside the material. From Fig. 19, it is estimated that $\tau_{max}\approx\mu/2.8\pi$ (for ν=0.3), i.e. the value of theoretical shear strength [1].

Purely gradient interface ($\mu_1=\mu_2$, $\nu_1=\nu_2$, $c_1\neq c_2$)

In this case, we consider the effects caused only by the difference in the gradient coefficients of the bonded media. Here we focus only on the "image" force F_x^{gr} which acts upon the dislocation due to the difference between the gradient coefficients c_1 and c_2. For a dislocation with Burgers vector b_x, this force is given (in units of $\mu_1 b_x^2/[\pi(k_1+1)]$) by [66]

$$F_x^{gr}(x') = 4\int_0^{+\infty} \frac{s^2}{\lambda_1+\lambda_2}\Big\{c_1(\lambda_2-\lambda_1)e^{-2x'\lambda_1} + (c_2-c_1)(\lambda_2-s)e^{-x'(\lambda_1+s)}\Big\}ds. \quad (64)$$

A numerical evaluation of this integral shows that F_x^{gr} is positive when $c_2>c_1$ and negative when $c_2<c_1$ (Fig. 20). This means that an edge dislocation is pushed away from the interface into the bulk of the material which has the smaller gradient coefficient, in contrast to the case of a screw dislocation (see Section 3.2.2) which exhibits opposite behavior. The reasons for this difference is not clear as yet. From Fig. 20, one can conclude that F_x^{gr} has a short-range character and acts just near the interface. At the interface, it attains a maximum value which depends strongly on the ratio c_2/c_1.

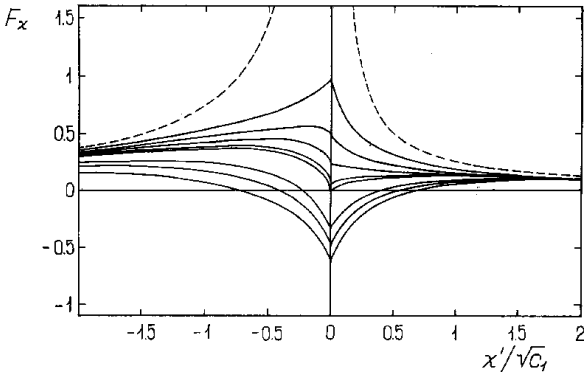

Fig. 17. The general "image" force F_x which acts upon the dislocation unit length due to the interface (at x=0) of two elastic media with $\mu_2=3\mu_1$ and c_2/c_1=0.3, 0.5, 0.7, 0.9, 1, 2, 3 and 5 (from top to bottom), as a function of the dislocation position $x'/\sqrt{c_1}$. The force values are given in units of $\mu_1 b_z^2/(2\pi\sqrt{c_1})$. The dashed curves represent the classical solution.

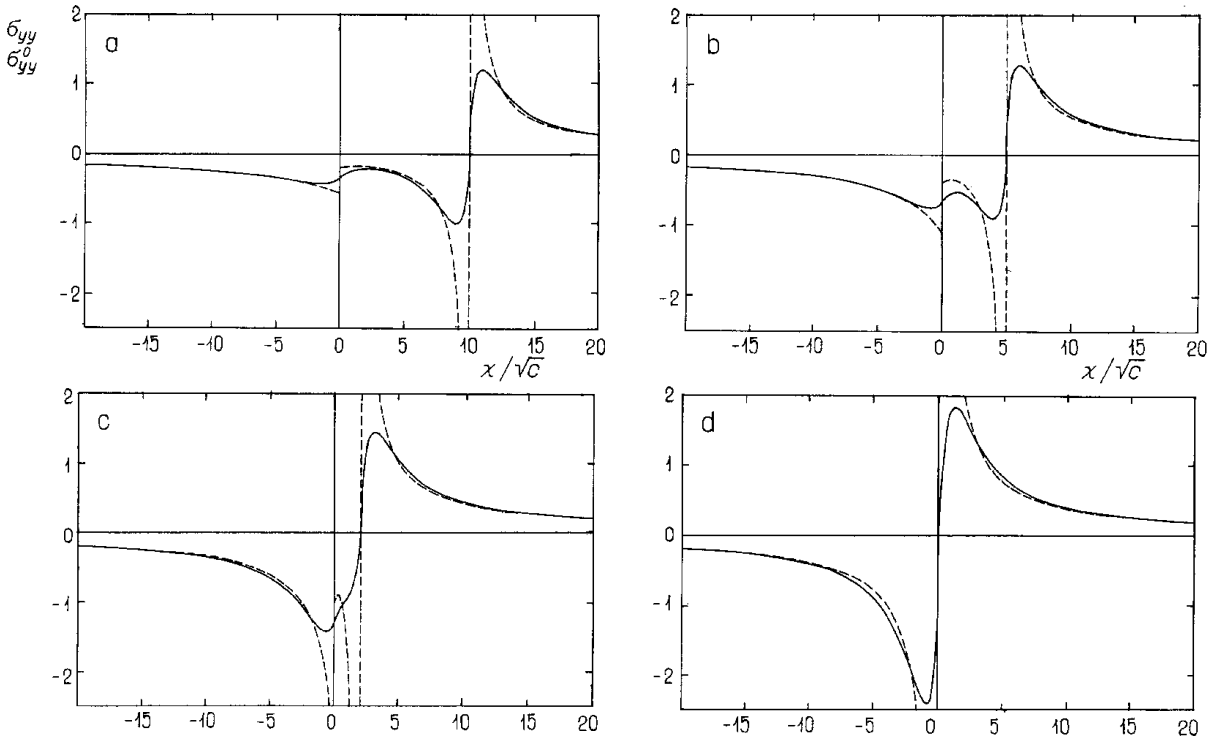

Fig. 18. The stress component $\sigma_{yy}(x,y=0)$ near the line of an edge dislocation with the Burgers vector b_y located at distances $x'/\sqrt{c}$ =10 (a), 5 (b), 2 (c) and 0 (d) from the interface (at x=0) of two elastic media with μ_2=10μ_1, ν_1=ν_2=0.3 and c_1=c_2=c. The stress values are given in units of $\mu_1 b_y/[\pi\,(k_1+1)\sqrt{c}\,]$. The dashed curves represent the classical solution σ_{yy}.

General mixed gradient elastic interface ($\mu_1\neq\mu_2$, $\nu_1\neq\nu_2$, $c_1\neq c_2$)

In this case, the "image" force F_x (in units of $\mu_1 b_x^2/[\pi(k_1+1)]$) is [66]

$$F_x(x') = -\frac{A+B}{2x'} + \frac{4Ac_1}{x'^3} + 4\int_0^{+\infty} \frac{s}{\lambda_1+\lambda_2}\Big[c_1 s(\lambda_2-\lambda_1)e^{-2x'\lambda_1} + \{B - Ac_1(\lambda_1^2+\lambda_2 s)(1+2x's) - c's(\lambda_2-s)\}e^{-x'(\lambda_1+s)}\Big]ds. \qquad (65)$$

It is worth noting that F_x is not a simple superposition of F_x^{el} and F_x^{gr} given by (63) and (64), respectively. This is illustrated in Fig. 21. The force in (65) is a nonsingular long-range force which is continuous across the interface and coincides with the classical solution far ($|x'|>5\sqrt{c_1}$) from the interface. Its values at the interface depend strongly on both ratios μ_2/μ_1 and c_2/c_1. In fact, the sign and qualitative behavior of F_x near the interface may be determined by c_2/c_1. For example, for μ_2/μ_1=3, there are three different types of behavior for F_x (Fig. 21). When $c_2>c_1$, $F_x>0$ everywhere and attains maximum values near or at the interface. When $c_2=c_1$, $F_x \equiv F_x^{el}$ (see above). When $c_2<c_1$, $F_x>0$ except at a very small region around the interface. Its size depends on c_2/c_1 and is about $0.3\sqrt{c_1}$; $F_x<0$ inside this region and attains minimum values at the interface. Thus, when $c_2\geq c_1$, the dislocation is pushed from material 2 into material 1 and possess no equilibrium position. When $c_2<c_1$ (e.g c_2/c_1=0.3), a dislocation being in material 2 is attracted to the interface and may be locked at a stable equilibrium position $x'\approx -0.1\sqrt{c_1}$ near the interface, while a dislocation located in material 1 possess an unstable equilibrium position $x'\approx 0.2\sqrt{c_1}$ near the interface; being attracted to it within a small region $x'<0.2\sqrt{c_1}$ and pushed away from the interface otherwise.

Thus, the gradient elasticity described by (5) has been employed to consider a straight dislocation near a flat interface which separates two elastic media with different elastic constants and gradient coefficients. We have derived [64-66], in integral forms, solutions for the dislocation stress fields and for the "image" force which acts upon the dislocation by the interface. It has been shown that all stress components remain continuous across the interface, in contrast to the well-known classical solution [69] where three (one for a screw dislocation and two for an edge dislocation) stress components suffer jump discontinuities there. Far from the interface and the dislocation line (at distances

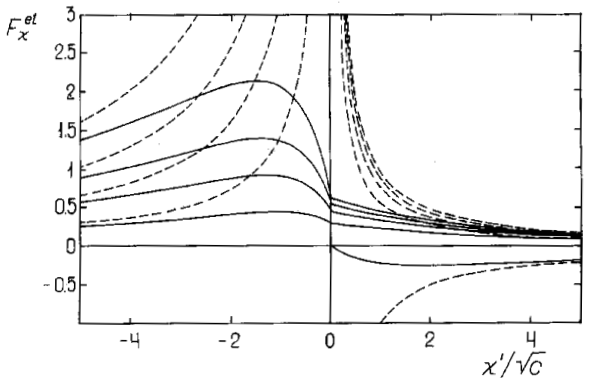

Fig. 19. The "image" force F_x^{el} which acts upon the dislocation unit length by the interface (at x=0) of two bonded media with c_1=c_2=c, ν_1=ν_2=0.3 and μ_2/μ_1=10, 7, 5, 3 and 0 (from top to bottom) as a function of the dislocation position $x'/\sqrt{c}$. The force values are given in units of $\mu_1 b_x^2/[\pi(k_1+1)\sqrt{c}]$. The dashed curves represent the classical solution.

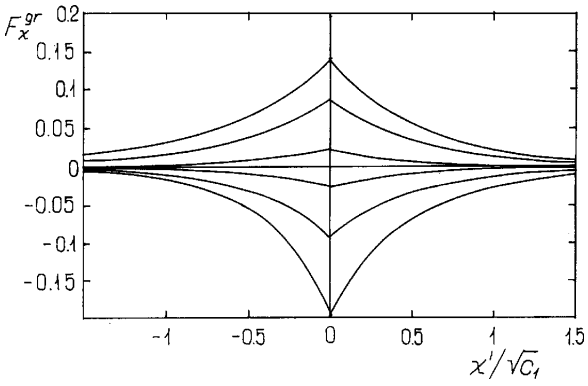

Fig. 20. The "image" force F_x^{gr} which acts upon the dislocation unit length by the interface (at x=0) of two bonded media with μ_2=μ_1, ν_1=ν_2=0.3 and c_2/c_1=2, 1.5, 1.1, 0.9, 0.7 and 0.5 (from top to bottom) as a function of the dislocation position $x'/\sqrt{c_1}$. The force values are given in units of $\mu_1 b_x^2/[\pi(k_1+1)\sqrt{c_1}]$.

>>$10\sqrt{c}$), gradient and classical solutions coincide. We have also dispensed with the classical singularity of the elastic "image" force acting upon the dislocation by the interface [69], and shown that it remains finite and continuous throughout. We have found an additional short-range elastic interaction between the dislocation and the interface due to the difference in the gradient coefficients of the media in contact. The additional "image" force acting upon the dislocation is finite and maximum at the interface. Under the action of this force, the screw (edge) dislocation tends to penetrate into the medium with the larger (smaller) gradient coefficient. In the general case where both the elastic constants μ_i and the gradient coefficients c_i are different for these media, the total "image" force exhibits quite different behavior near the interface depending on the ratios μ_2/μ_1 and c_2/c_1, while its long-range component remains as in the classical theory of elasticity.

4. NANOSCALE ELASTIC PROPERTIES OF DISCLINATIONS

In considering straight disclinations, it is reasonable to start from the solutions for the so-called screened disclination configurations [7, 12] because the classical elastic fields for individual disclinations in infinite media contain the terms which are singular at infinity (~ $r\ln r$ for displacements, ~ $\ln r$ for strains and stresses) and have no physical meaning (dimensional quantities under the logarithm signs). Among the various screened disclination configurations, we have chosen that of disclination dipoles not only because they are described by simple expressions in classical elasticity [5-7] but also because they are very convenient to determine elastic interactions. Thus, the gradient solutions have been originally obtained for a disclination dipole within both the gradient theories described by (4) [58] and (5) [62, 63]. For shorteness, we present below the general solution for an individual disclination obtained as a limiting case of a disclination dipole [58, 62, 63]. However, we also consider disclination dipoles in Section 4.2 to discuss mostly important features of the gradient solution.

4.1. Individual disclinations – a general solution

Consider a disclination of general type with Frank vector $\boldsymbol{\omega}$= $\omega_x \boldsymbol{e}_x + \omega_y \boldsymbol{e}_y + \omega_z \boldsymbol{e}_z$ in an infinite elastic medium. The scalars ω_x and ω_y determine the twist components of the disclination while ω_z determines its wedge component. Let its line coincides with the z-axis of the Carthesian coordinate system and the Frank vector is applied at the origin of this coordinate system. For such an isolated disclination, both classical and gradient solutions themselves have no physical meaning because they are not screened but they may be used in modelling screened disclination configurations as basic elements [7, 12].

Classical solution

The classical solution for elastic strain fields ε_{ij}^0 reads [5-7] (in units of $1/[4\pi(1-\nu)]$)

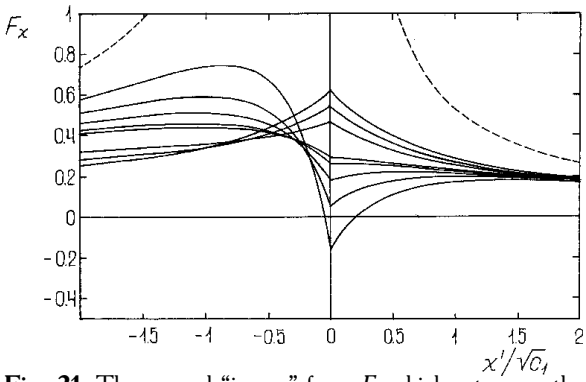

Fig. 21. The general "image" force F_x which acts upon the dislocation unit length by the interface (at $x=0$) of two bonded media with $\mu_2=3\mu_1$, $\nu_1=\nu_2=0.3$ and $c_2/c_1=5$, 3, 2, 1, 0.9, 0.7, 0.5 and 0.3 (from top to bottom) as a function of the dislocation position $x'/\sqrt{c_1}$. The force values are given in units of $\mu_1 b_x^2/[\pi(k_1+1)\sqrt{c_1}]$. The dashed curves represent the classical solution.

$$\varepsilon^0_{xx}=\omega_x zx\frac{2\nu r^2-x^2+y^2}{r^4}+\omega_y zy\frac{2\nu r^2-3x^2-y^2}{r^4}$$
$$+\omega_z\left\{(1-2\nu)\ln r+\frac{y^2}{r^2}\right\},$$

$$\varepsilon^0_{yy}=\omega_x zx\frac{2\nu r^2-x^2-3y^2}{r^4}+\omega_y zy\frac{2\nu r^2+x^2-y^2}{r^4}$$
$$+\omega_z\left\{(1-2\nu)\ln r+\frac{x^2}{r^2}\right\},$$

$$\varepsilon^0_{xy}=(\omega_y x-\omega_x y)z\frac{x^2-y^2}{r^4}-\omega_z\frac{xy}{r^2},\qquad(66)$$

$$\varepsilon^0_{xz}=\omega_y\frac{xy}{r^2}-\omega_x\left\{(1-2\nu)\ln r+\frac{y^2}{r^2}\right\},$$

$$\varepsilon^0_{yz}=\omega_x\frac{xy}{r^2}-\omega_y\left\{(1-2\nu)\ln r+\frac{x^2}{r^2}\right\},$$

and for the stress fields it may be written (in units of $\mu/[2\pi(1-\nu)]$) as

$$\sigma^0_{xx}=\varepsilon^0_{xx}(\nu=0),\ \sigma^0_{yy}=\varepsilon^0_{yy}(\nu=0),$$
$$\sigma^0_{xy}=\varepsilon^0_{xy},\quad \sigma^0_{xz}=\varepsilon^0_{xz},\quad \sigma^0_{yz}=\varepsilon^0_{yz},$$
$$\sigma^0_{zz}=-\omega_z z2\nu\frac{x}{r^2}-\omega_y z2\nu\frac{y}{r^2}+\omega_z 2\nu\ln r,\qquad(67)$$

where $r^2=x^2+y^2$. Most of the components in (66) and (67) contain singular terms $\sim\ln r$.

Gradient solution

The gradient solutions have been originally obtained for a disclination dipole within both the gradient theories described by (4) [58] and (5) [62, 63]. Solving (7), we have finally for an individual disclination under consideration the strain field $\varepsilon_{ij}=\varepsilon^0_{ij}+\varepsilon^{gr}_{ij}$, where ε^0_{ij} are given by (66) and ε^{gr}_{ij} (in units of $1/[4\pi(1-\nu)]$) by [58, 62, 63]

$$\varepsilon^{gr}_{xx}=\omega_x 2xz\left\{(y^2-\nu r^2)\Phi_1+(x^2-3y^2)\Phi_2\right\}$$
$$+\omega_y 2yz\left\{(y^2-\nu r^2)\Phi_1+(3x^2-y^2)\Phi_2\right\}$$
$$+\omega_z\left\{\Phi_0+r^2(x^2-y^2)\Phi_2\right\},$$

$$\varepsilon^{gr}_{yy}=\omega_x 2xz\left\{(x^2-\nu r^2)\Phi_1-(x^2-3y^2)\Phi_2\right\}$$
$$+\omega_y 2yz\left\{(x^2-\nu r^2)\Phi_1-(3x^2-y^2)\Phi_2\right\}$$
$$+\omega_z\left\{\Phi_0-r^2(x^2-y^2)\Phi_2\right\},$$

$$\varepsilon^{gr}_{xy}=\omega_x 2yz\left\{-x^2\Phi_1+(3x^2-y^2)\Phi_2\right\}$$
$$-\omega_y 2xz\left\{y^2\Phi_1+(x^2-3y^2)\Phi_2\right\}+\omega_z 2xyr^2\Phi_2,\qquad(68)$$

$$\varepsilon^{gr}_{xz}=\omega_z\left\{-\Phi_0-r^2(x^2-y^2)\Phi_2\right\}-\omega_y 2xyr^2\Phi_2,$$

$$\varepsilon^{gr}_{yz}=\omega_y\left\{-\Phi_0+r^2(x^2-y^2)\Phi_2\right\}-\omega_x 2xyr^2\Phi_2,$$

where Φ_i are the same as in Section 3.1.1. For the stress field, the solution of (8) gives $\sigma_{ij}=\sigma^0_{ij}+\sigma^{gr}_{ij}$, where σ^0_{ij} are given by (67) and σ^{gr}_{ij} (in units of $\mu/[2\pi(1-\nu)]$) by [62, 63]

$$\sigma^{gr}_{xx}=\varepsilon^{gr}_{xx}(\nu=0,c_2\leftrightarrow c_1),$$
$$\sigma^{gr}_{yy}=\varepsilon^{gr}_{yy}(\nu=0,c_2\leftrightarrow c_1),$$
$$\sigma^{gr}_{zz}=2\nu\{(\omega_x x+\omega_y y)zr^2\Phi_1(c_2\leftrightarrow c_1)$$
$$+\omega_z\Phi_0(\nu=0,c_2\leftrightarrow c_1)\},$$
$$\sigma^{gr}_{xy}=\varepsilon^{gr}_{xy}(c_2\leftrightarrow c_1),\qquad(69)$$
$$\sigma^{gr}_{xz}=\varepsilon^{gr}_{xz}(c_2\leftrightarrow c_1),$$
$$\sigma^{gr}_{yz}=\varepsilon^{gr}_{yz}(c_2\leftrightarrow c_1).$$

Using the limiting transitions noted in Section 3.1.1, it is easily to show the total elimination of classical logarithmic singularity from elastic fields (68) and (69). In the next sections we consider similar elastic fields of disclination dipoles in detail and discuss their characteristic features separately for twist disclinations of two types as well as for wedge disclinations.

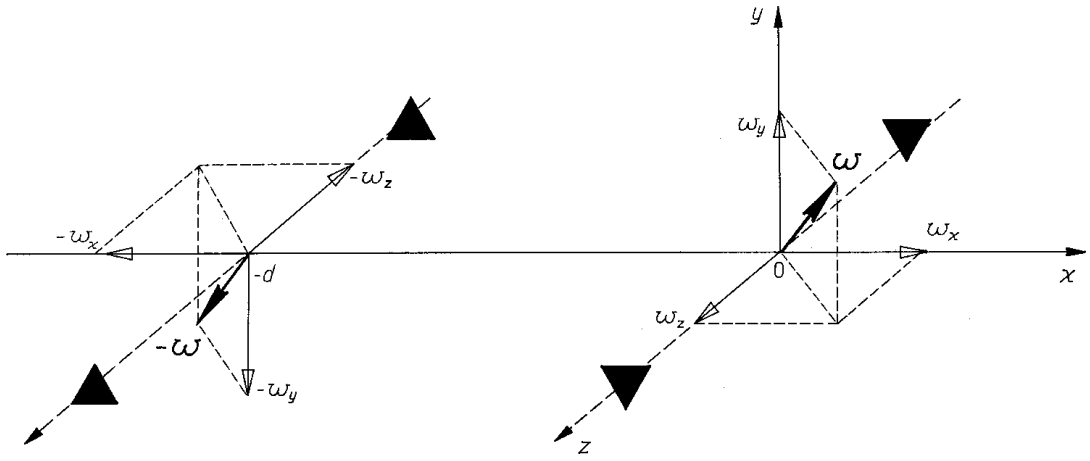

Fig. 22. A dipole of straight disclinations having the Frank vectors $\pm\boldsymbol{\omega}$.

4.2. Disclination dipoles

We discuss below two interesting aspects, i.e. the behavior of elastic strains near disclination lines and the short-range elastic interaction between disclinations in a dipole. It is more convenient to discuss twist and wedge disclinations separately.

Consider a disclination dipole which consists of two parallel disclinations with Frank vector $\pm\boldsymbol{\omega}$ ($\boldsymbol{\omega} = \omega_x \boldsymbol{e}_x + \omega_y \boldsymbol{e}_y + \omega_z \boldsymbol{e}_z$). The scalars ω_x and ω_y determine the twist components of the disclinations while ω_z determines their wedge component (Fig. 22). Let the disclinations lie in the plane y=0 along the z-axis and cross the x-axis at the points x=-d (negative disclination) and x=0 (positive disclination).

4.2.1. First-type twist disclinations

We consider here a dipole of twist disclinations having the Frank vectors $\pm\boldsymbol{\omega}$=($\pm\omega_x$,0,0). The elastic strain (stress) components of such a dipole are given by the simple superpositions of the terms associated with ω_x in (66) and (68) ((67) and (69)), and similar terms taken with the opposite sign [58, 63].

Let us discuss first the behavior of the elastic strains and stresses near the line of the positive disclination (x=0, y=0). For $r\to 0$ we have for strains (in units of $\omega_x/[4\pi(1\text{-}\nu)]$) [58]

$$\varepsilon_{xx}|_{r\to 0} = z\left\{\frac{1-2\nu}{d} - \frac{4c_2}{d^3} + \frac{2\nu}{\sqrt{c_2}} K_1\left(\frac{d}{\sqrt{c_2}}\right) + \frac{2}{d} K_2\left(\frac{d}{\sqrt{c_2}}\right)\right\},$$

$$\varepsilon_{yy}|_{r\to 0} = z\left\{\frac{1-2\nu}{d} + \frac{4c_2}{d^3} - \frac{2(1-\nu)}{\sqrt{c_2}} K_1\left(\frac{d}{\sqrt{c_2}}\right) - \frac{2}{d} K_2\left(\frac{d}{\sqrt{c_2}}\right)\right\},$$

$$\varepsilon_{xy}|_{r\to 0} = \varepsilon_{yz}|_{r\to 0} = 0, \qquad (70)$$

$$\varepsilon_{xz}|_{r\to 0} = -\frac{1}{2} + (1-2\nu) + \left(\gamma + \ln\frac{d}{2\sqrt{c_2}}\right) + \frac{2c_2}{d^2} + (1-2\nu) K_0\left(\frac{d}{\sqrt{c_2}}\right) - K_2\left(\frac{d}{\sqrt{c_2}}\right),$$

$$\varepsilon|_{r\to 0} = 2(1-2\nu) z\left\{\frac{1}{d} - \frac{1}{\sqrt{c_2}} K_1\left(\frac{d}{\sqrt{c_2}}\right)\right\},$$

and for stresses (in units of $\mu\omega_x/[2\pi(1\text{-}\nu)]$) [63]

$$\begin{aligned}
&\sigma_{xx}|_{r\to 0} = \varepsilon_{xx}(\nu = 0, c_2 \leftrightarrow c_1)|_{r\to 0}, \\
&\sigma_{yy}|_{r\to 0} = \varepsilon_{yy}(\nu = 0, c_2 \leftrightarrow c_1)|_{r\to 0}, \\
&\sigma_{zz}|_{r\to 0} = z2\nu\left\{\frac{1}{d} - \frac{1}{\sqrt{c_1}} K_1\left(\frac{d}{\sqrt{c_1}}\right)\right\}, \qquad (71) \\
&\sigma_{xy}|_{r\to 0} = \sigma_{yz}|_{r\to 0} = 0, \\
&\sigma_{xz}|_{r\to 0} = \varepsilon_{xz}(c_2 \leftrightarrow c_1)|_{r\to 0},
\end{aligned}$$

It is seen that the elastic strains and stresses are finite at the disclination line in contrast to the classical

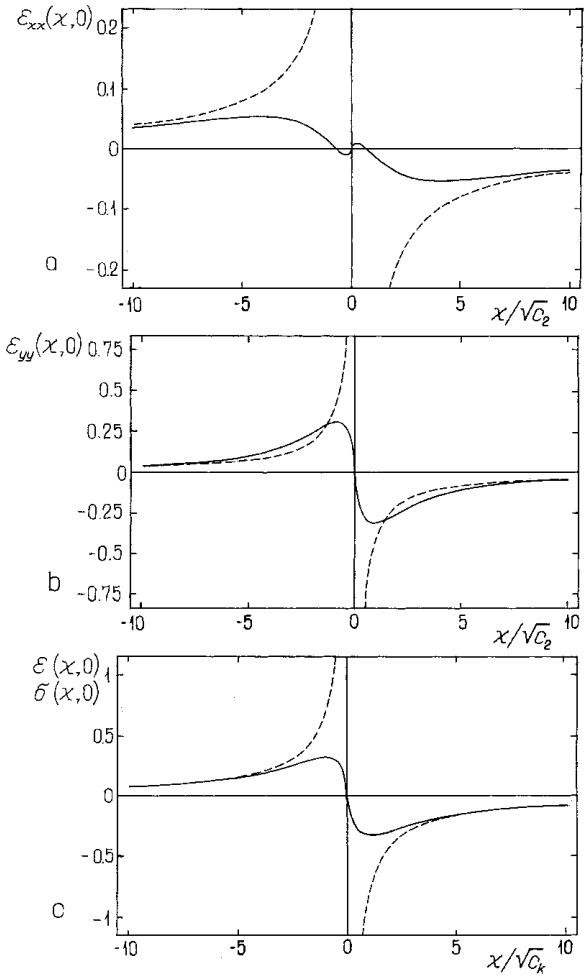

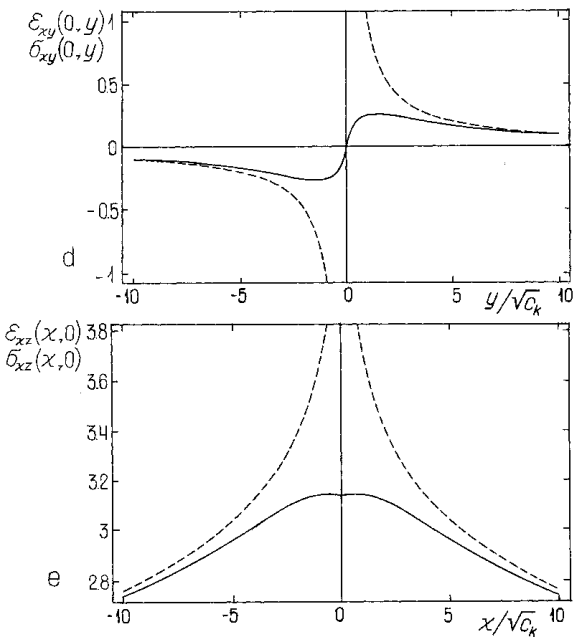

Fig. 23. The components of strains $\varepsilon_{xx}(x,0)$ – (a); $\varepsilon_{yy}(x,0)$ – (b); $\varepsilon(x,0)$ – (c); $\varepsilon_{xy}(0,y)$ – (d); $\varepsilon_{xz}(x,0)$ (e); and stresses $\sigma(x,0)$ – (c); $\sigma_{xy}(0,y)$ – (d); $\sigma_{xz}(x,0)$ – (e) near the line of the positive first-type twist disclination when the dipole arm $d=10^4\sqrt{c_k}$. The strain values are given in units of $\omega_x z/[4\pi(1-\nu)\sqrt{c_2}]$ – (a-d) and $\omega_x/[4\pi(1-\nu)]$ – (e), and the stress values, in units of $\mu\omega_x z(1+\nu)/[6\pi(1-\nu)(1-2\nu)\sqrt{c_1}]$ – (c); $\mu\omega_x z/[2\pi(1-\nu)\sqrt{c_1}]$ – (d), and $\mu\omega_x/[2\pi(1-\nu)]$ –(e). The dashed curves represent the classical solutions ε_{ij}^0 and σ_{ij}^0.

solutions (66) and (67), respectively, which are singular there. The values of the strain and stress components at the disclination line depend, in general, on the dipole arm d.

For $d >> \sqrt{c_2}$ (long-range disclination interaction), the strain components read (in units of $\omega_x/[4\pi(1-\nu)]$) [58]

$$\begin{aligned}
&\varepsilon_{xx}|_{r\to 0} = \varepsilon_{yy}|_{r\to 0} = \frac{\varepsilon}{2}|_{r\to 0} = (1-2\nu)\frac{z}{d},\\
&\varepsilon_{xy}|_{r\to 0} = \varepsilon_{yz}|_{r\to 0} = 0,\\
&\varepsilon_{xz}|_{r\to 0} = -\frac{1}{2} + (1-2\nu)\left(\gamma + \ln\frac{d}{2\sqrt{c_2}}\right),
\end{aligned} \tag{72}$$

and the stress components are (in units of $\mu\omega_x/[2\pi(1-\nu)]$)

$$\begin{aligned}
&\sigma_{xx}|_{r\to 0} = \sigma_{yy}|_{r\to 0} = \sigma_{zz}|_{r\to 0}/(2\nu) = \frac{z}{d},\\
&\sigma_{xy}|_{r\to 0} = \sigma_{yz}|_{r\to 0} = 0,\\
&\sigma_{xz}|_{r\to 0} = \varepsilon_{xz}(c_2 \leftrightarrow c_1)|_{r\to 0}.
\end{aligned} \tag{73}$$

Fig. 23 provides the distribution of elastic strains and stresses in the planes y=0 (Fig. 23a-c, e) and x=0 (Fig. 23d) near the line of the positive disclination located at the point (0,0) of Fig. 22 when $d=10^4\sqrt{c_k}$, where k=1 for stresses and k=2 for strains [58, 63]. The solid lines represent the gradient solution while the dashed lines represent the classical one. One can see that within the gradient elasticity, the elastic strains and stresses are finite and much smaller near the disclination line, they achieve extreme values there and tend to the classical solution at distances far away from the disclination line ($r>5\sqrt{c_k}$).

A general view on the distribution of elastic strains and stresses given by the classical and gradient elasticity, is provided in Fig. 24. The top pictures represent the classical solution, while the bottom pictures represent the gradient solution. Fig. 24 clearly illustrates the elimination of classical singularities near the disclination line within the gradient theory.

The absence of classical singularities permits to investigate short-range elastic interactions between disclinations. For example, one can observe the strained states at two characteristic points of the disclination

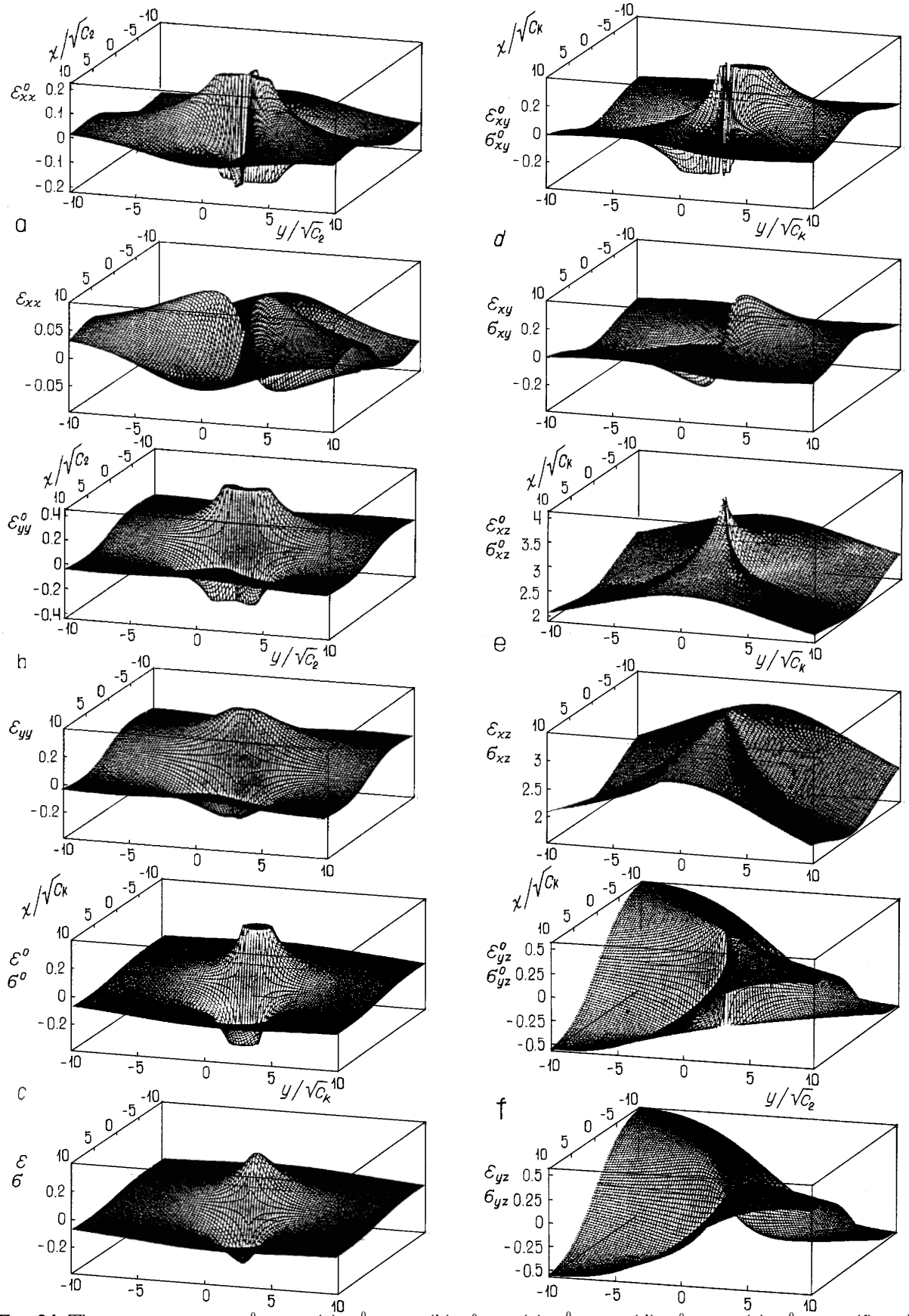

Fig. 24. The strain components ε^0_{xx}, ε_{xx} – (a); ε^0_{yy}, ε_{yy} – (b); ε^0, ε – (c); ε^0_{xy}, ε_{xy} – (d); ε^0_{xz}, ε_{xz} – (e); ε^0_{yz}, ε_{yz} – (f); and stresses σ^0, σ – (c); σ^0_{xy}, σ_{xy} – (d); σ^0_{xz}, σ_{xz} – (e); σ^0_{yz}, σ_{yz} – (f), near the line of the positive first-type twist disclination when the dipole arm $d=10^4\sqrt{c_k}$. The strain values are given in units of $\omega_x z/[4\pi(1-\nu)\sqrt{c_2}]$ – (a-d) and $\omega_x/[4\pi(1-\nu)]$ – (e,f), and the stress values, in units of $\mu\omega_x z(1+\nu)/[6\pi(1-\nu)(1-2\nu)\sqrt{c_1}]$ – (c); $\mu\omega_x z/[2\pi(1-\nu)\sqrt{c_1}]$ – (d), and $\mu\omega_x/[2\pi(1-\nu)]$ – (e,f). The top figures give the classical solutions ε^0_{ij} and σ^0_{ij} while the bottom ones give the gradient solutions ε_{ij} and σ_{ij}.

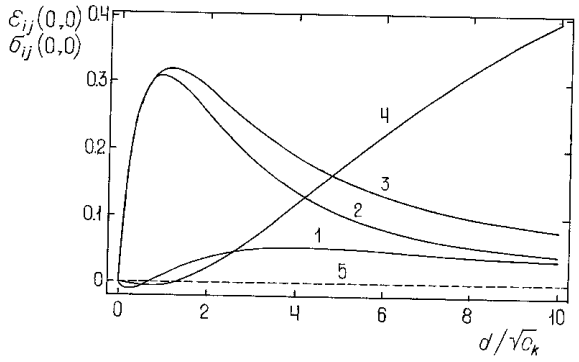

Fig. 25. The strain (stress) components ε_{xx} – (1), ε_{yy} – (2), $\varepsilon(\sigma)$ – (3), $\varepsilon_{xz}(\sigma_{xz})$ – (4), and $\varepsilon_{xy}(\sigma_{xy})= \varepsilon_{yz}(\sigma_{yz})=0$ – (5) at the line of the positive first-type twist disclination via the dipole arm d. The dashed line (5) gives the zero level. The strain values are given in units of $\omega_x z/[4\pi(1\text{-}\nu)\sqrt{c_2}]$ – (1–3) and $\omega_x/[4\pi(1\text{-}\nu)]$ – (4), while the stress values, in units of $\mu\omega_x z(1+\nu)/[6\pi(1\text{-}\nu)(1\text{-}2\nu)\sqrt{c_1}]$ – (3) and $\mu\omega_x/[2\pi(1\text{-}\nu)]$ – (4).

dipole, e.g. at the disclination line (0,0) and at the middle of the dipole (-d/2,0). In the first case, one can use Eqs. 70 and 71 which are represented graphically in Fig. 25. It is seen that the elastic strains and stresses vary non-monotonously with the variation of d within this interval and they are strictly equal to zero at d=0 (annihilation of disclinations). A similar conclusion may be drawn in the second case (Fig. 26). When $d>>\sqrt{c_k}$, the strains and hydrostatic stress decrease monotonously with increasing d, i.e. the characteristic behavior for the long-range disclination interaction for the gradient solution is the same as for the classical solution. When $d<10\sqrt{c_k}$, the strains and hydrostatic stress vary non-monotonously with d and becomes exactly zero at d=0, in contrast to the classical solution which gives a monotonous singular dependence on d.

4.2.2. Second-type twist disclinations

Next, we consider a dipole of twist disclinations having the Frank vectors $\pm\boldsymbol{\omega}=(0,\pm\omega_y,0)$. The elastic strain (stress) components of such a dipole are given by the simple superpositions of the terms associated with ω_y in (66) and (68) ((67) and (69)), and similar terms taken with the opposite sign [58, 63].

Near the line of the positive disclination, at $r\to 0$, we have for strains (in units of $\omega_y/[4\pi(1\text{-}\nu)]$) [58]

$$\varepsilon_{xx}|_{r\to 0} = \varepsilon_{yy}|_{r\to 0} = \varepsilon|_{r\to 0} = \varepsilon_{xz}|_{r\to 0} = 0,$$
$$\varepsilon_{xy}|_{r\to 0} = z\left\{-\frac{1}{d}+\frac{4c_2}{d^3}-\frac{2}{d}K_2\left(\frac{d}{\sqrt{c_2}}\right)\right\},$$

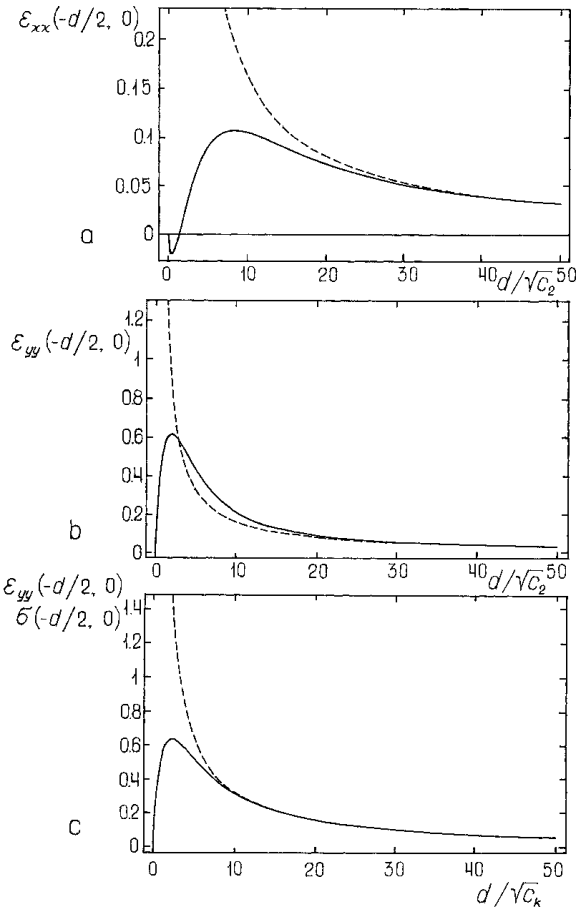

Fig. 26. The strain (hydrostatic stress) components ε^0_{xx}, ε_{xx} – (a), ε^0_{yy}, ε_{yy} – (b), and ε^0, $\varepsilon(\sigma^0,\sigma)$ – (c) in the middle of the dipole of first-type twist disclinations (the point $(-d/2,0)$) via the dipole arm d. The dashed curves represent the classical solution $\varepsilon^0_{ij}(\sigma^0_{ij})$. The strain values are given in units of $\omega_x z/[4\pi(1\text{-}\nu)\sqrt{c_2}]$, while the stress values, in units of $\mu\omega_x z(1+\nu)/[6\pi(1\text{-}\nu)(1\text{-}2\nu)\sqrt{c_1}]$.

$$\varepsilon_{yz}|_{r\to 0} = \frac{1}{2}+(1-2\nu)\left(\gamma+\ln\frac{d}{2\sqrt{c_2}}\right)- \frac{2c_2}{d^2}+(1-2\nu)K_0\left(\frac{d}{\sqrt{c_2}}\right)+K_2\left(\frac{d}{\sqrt{c_2}}\right), \tag{74}$$

and for stresses (in units of $\mu\omega_y/[2\pi(1\text{-}\nu)]$) [63]

$$\sigma_{xx}|_{r\to 0} = \sigma_{yy}|_{r\to 0} = \sigma_{zz}|_{r\to 0} = \sigma_{xz}|_{r\to 0} = 0,$$
$$\sigma_{xy}|_{r\to 0} = \varepsilon_{xy}(c_2 \leftrightarrow c_1)|_{r\to 0}, \tag{75}$$
$$\sigma_{yz}|_{r\to 0} = \varepsilon_{yz}(c_2 \leftrightarrow c_1)|_{r\to 0}.$$

We see again that the elastic strains and stresses are finite at the disclination line, in contrast to the classical solutions (66) and (67) which are singular there. The values of the strain (stress) components ε_{xy} and ε_{yz} (σ_{xy} and σ_{yz}) at the disclination line depend on the dipole arm d.

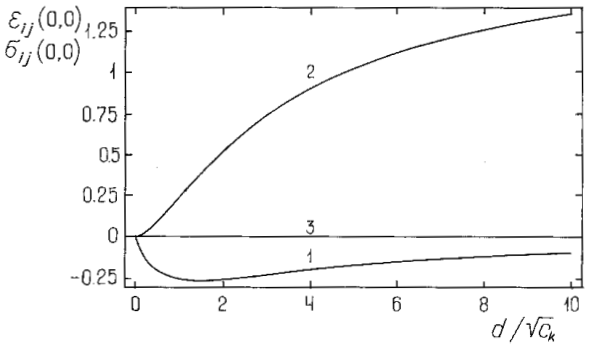

Fig. 27. The strain (stress) components $\varepsilon_{xy}(\sigma_{xy})$ – (1), $\varepsilon_{yz}(\sigma_{yz})$ – (2), and $\varepsilon_{xx}(\sigma_{xx})=\varepsilon_{yy}(\sigma_{yy})=\varepsilon(\sigma)=\varepsilon_{xz}(\sigma_{xz})=0$ – (3) at the line of the positive second-type twist disclination via then dipole arm d. The strain values are given in units of $\omega_y z/[4\pi(1\text{-}\nu)\sqrt{c_2}]$ – (1) and $\omega_y/[4\pi(1\text{-}\nu)]$ – (2), while the stress values, in units of $\mu\omega_y z/[2\pi(1\text{-}\nu)\sqrt{c_1}]$ – (1) and $\mu\omega_y[2\pi(1\text{-}\nu)]$ – (2).

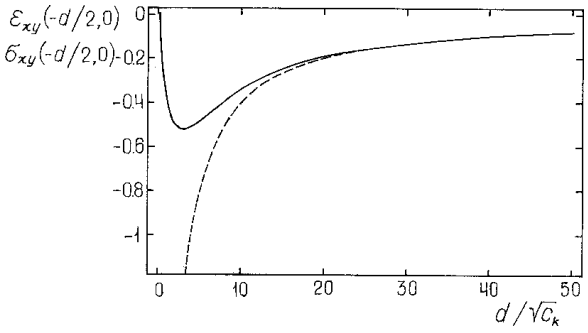

Fig. 28. The only non-vanishing strain (stress) components $\varepsilon^0_{xy}(\sigma^0_{xy})$ (the dashed curve) and $\varepsilon_{xy}(\sigma_{xy})$ (the solid curve) in the middle of the dipole of second-type twist disclinations (the point $(-d/2,0)$) via the dipole arm d. The strain values are given in units of $\omega_y z/[4\pi(1\text{-}\nu)\sqrt{c_2}]$, while the stress values, in units of $\mu\omega_y z/[2\pi(1\text{-}\nu)\sqrt{c_1}]$.

For $d>>\sqrt{c_k}$ (long-range disclination interaction), the strain components read (in units of $\omega_y/[4\pi(1\text{-}\nu)]$) [58]

$$\begin{aligned}
&\varepsilon_{xx}|_{r\to 0} = \varepsilon_{yy}|_{r\to 0} = \varepsilon|_{r\to 0} = \varepsilon_{xz}|_{r\to 0} = 0,\\
&\varepsilon_{xy}|_{r\to 0} = -\frac{z}{d},\\
&\varepsilon_{yz}|_{r\to 0} = \frac{1}{2} + (1-2\nu)\left(\gamma + \ln\frac{d}{2\sqrt{c_2}}\right),
\end{aligned} \tag{76}$$

and the stress components are (in units of $\mu\omega_y/[2\pi(1\text{-}\nu)]$)

$$\begin{aligned}
&\sigma_{xx}|_{r\to 0} = \sigma_{yy}|_{r\to 0} = \sigma_{zz}|_{r\to 0} = \sigma_{xz}|_{r\to 0} = 0,\\
&\sigma_{xy}|_{r\to 0} = -\frac{z}{d},\\
&\sigma_{yz}|_{r\to 0} = \varepsilon_{yz}(c_2 \leftrightarrow c_1)|_{r\to 0}.
\end{aligned} \tag{77}$$

The distribution of elastic strains and stresses near the disclination line in this case is similar to the case considered in the previous subsection. In fact, since in the limiting case of large d, the strain (stress) components for the ω_x-disclination transform into the strain (stress) components for the ω_y-disclination by the simple interchange of x and y, Fig. 23a may be viewed as representing the strain (stress) component $\varepsilon_{yy}(0,y)$, Fig. 23b – $\varepsilon_{xx}(0,y)$, Fig. 23c – $\varepsilon(0,y)(\sigma(0,y))$, Fig. 23d – $\varepsilon_{xy}(x,0)(\sigma_{xy}(x,0))$, and Fig. 23e – $\varepsilon_{yz}(0,y)(\sigma_{yz}(0,y))$, with the appropriate substitution of ω_x by ω_y in the measured units. In this case, the solid lines represent the gradient solution, while the dashed lines represent the classical one.

In a similar way, the general view on the distribution of elastic strains and stresses given by classical and gradient elasticity for ω_y-disclinations, may be seen in Fig. 24 with the interchange of x- and y-axes. As a result, Fig. 24a may represent the strain component ε_{yy}, Fig. 24b – ε_{xx}, Fig. 24c – $\varepsilon(\sigma)$, Fig. 24d – $\varepsilon_{xy}(\sigma_{xy})$, Fig. 24e – $\varepsilon_{yz}(\sigma_{yz})$, and Fig. 24f – $\varepsilon_{xz}(\sigma_{xz})$, with the appropriate substitution of ω_x by ω_y in the measured units. The top pictures represent again the classical solution, while the bottom pictures represent the gradient solution.

In this case also, the absence of classical singularities permits to investigate short-range elastic interactions between disclinations. Again, one can observe the strained states at two characteristic points of the disclination dipole, i.e. at the disclination line (0,0) and at the middle of the dipole $(-d/2,0)$. In the first case, one can use Eqs. 74 and 75 which are represented graphically in Fig 27. Two non-vanishing strain (stress) components $\varepsilon_{xy}(\sigma_{xy})$ – (1) and $\varepsilon_{yz}(\sigma_{yz})$ – (2) vary non-monotonously with the variation of d within the interval $d<10\sqrt{c_k}$ and are equal to zero at $d=0$ (annihilation of disclinations). A similar conclusion may be drawn in the second case (Fig. 28) for the only one non-vanishing strain (stress) component $\varepsilon_{xy}(\sigma_{xy})$. When $d>>\sqrt{c_k}$, the strain (stress) values decrease monotonously with increasing d, i.e. the characteristic behavior for the long-range disclination interaction for the gradient solution is the same as for the classical solution. When $d<10\sqrt{c_k}$, the strain (stress) varies non-monotonously with d and is equal to zero at $d=0$, in contrast to the classical solution which gives a monotonous singular dependence on d.

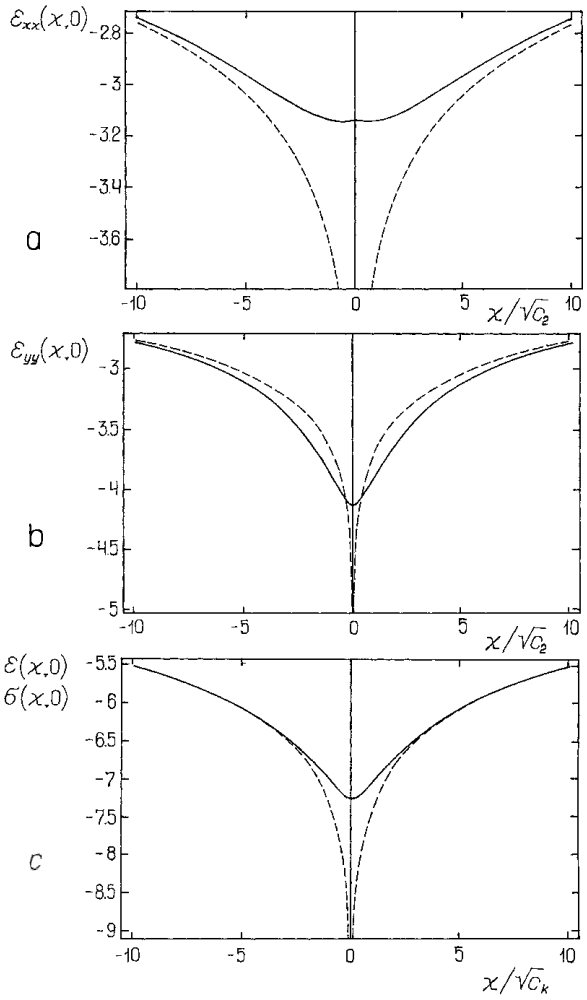

Fig. 29. The strain (hydrostatic stress) components $\varepsilon_{xx}(x,0)$ – (a), $\varepsilon_{yy}(x,0)$ – (b), and $\varepsilon(x,0)(\sigma(x,0))$ – (c) near the line of the positive wedge disclination when the dipole arm $d=10^4\sqrt{c_k}$. The strain values are given in units of $\omega_z/[4\pi(1-\nu)]$, while the stress values, in units of $\mu\omega_z(1+\nu)/[6\pi(1-\nu)(1-2\nu)]$. The dashed curves represent the classical solutions ε^0_{ij} (σ^0).

4.2.3. Wedge disclinations

Consider a dipole of wedge disclinations having the Frank vectors $\pm\boldsymbol{\omega}=(0,0,\pm\omega_z)$. The elastic strain (stress) components of such a dipole are given by the simple superpositions of the terms associated with ω_z in (66) and (68) ((67) and (69)), and similar terms taken with the opposite sign [58, 63].

Near the line of the positive disclination, at $r\to 0$, the strains result in (in units of $\omega_z/[4\pi(1-\nu)]$) [58]

$$\varepsilon_{xx}|_{r\to 0}=\frac{1}{2}-(1-2\nu)\left(\gamma+\ln\frac{d}{2\sqrt{c_2}}\right)-\frac{2c_2}{d^2}$$
$$-(1-2\nu)K_0\left(\frac{d}{\sqrt{c_2}}\right)+K_2\left(\frac{d}{\sqrt{c_2}}\right),$$

$$\varepsilon_{yy}|_{r\to 0}=-\frac{1}{2}-(1-2\nu)\left(\gamma+\ln\frac{d}{2\sqrt{c_2}}\right)+\frac{2c_2}{d^2}$$
$$-(1-2\nu)K_0\left(\frac{d}{\sqrt{c_2}}\right)-K_2\left(\frac{d}{\sqrt{c_2}}\right), \qquad (78)$$

$$\varepsilon_{xy}|_{r\to 0}=0,$$

$$\varepsilon|_{r\to 0}=-2(1-2\nu)\left\{\gamma+\ln\frac{d}{2\sqrt{c_2}}+K_0\left(\frac{d}{\sqrt{c_2}}\right)\right\},$$

and the stresses are given (in units of $\mu\omega_z/[2\pi(1-\nu)]$) by [63]

$$\sigma_{xx}|_{r\to 0}=\varepsilon_{xx}(\nu=0,c_2\leftrightarrow c_1)|_{r\to 0},$$
$$\sigma_{yy}|_{r\to 0}=\varepsilon_{yy}(\nu=0,c_2\leftrightarrow c_1)|_{r\to 0},$$
$$\sigma_{xy}|_{r\to 0}=\varepsilon_{xy}(c_2\leftrightarrow c_1)|_{r\to 0}, \qquad (79)$$
$$\sigma_{zz}|_{r\to 0}=-2\nu\left\{\gamma+\ln\frac{d}{2\sqrt{c_1}}+K_0\left(\frac{d}{\sqrt{c_1}}\right)\right\}.$$

One can see that the elastic strains and stresses are finite at the wedge disclination line as is the case with twist disclinations, in contrast to the classical solutions (66) and (67) which are singular there. The values of the strain and stress components at the disclination line depend again on the dipole arm d.

For $d>>\sqrt{c_k}$ (long-range disclination interaction), the strain components transform (in units of $\omega_z/[4\pi(1-\nu)]$) into [58]

$$\varepsilon_{xx}|_{r\to 0}=\frac{1}{2}-(1-2\nu)\left(\gamma+\ln\frac{d}{2\sqrt{c_2}}\right),$$
$$\varepsilon_{yy}|_{r\to 0}=-\frac{1}{2}-(1-2\nu)\left(\gamma+\ln\frac{d}{2\sqrt{c_2}}\right),$$
$$\varepsilon_{xy}|_{r\to 0}=0, \qquad (80)$$
$$\varepsilon|_{r\to 0}=-2(1-2\nu)\left(\gamma+\ln\frac{d}{2\sqrt{c_2}}\right),$$

and the stress components are (in units of $\mu\omega_z/[2\pi(1-\nu)]$)

$$\sigma_{xx}|_{r\to 0} = \varepsilon_{xx}(\nu = 0, c_2 \leftrightarrow c_1)|_{r\to 0},$$
$$\sigma_{yy}|_{r\to 0} = \varepsilon_{yy}(\nu = 0, c_2 \leftrightarrow c_1)|_{r\to 0}$$
$$\sigma_{xy}|_{r\to 0} = 0,$$
$$\sigma_{zz}|_{r\to 0} = -2\nu\left(\gamma + \ln\frac{d}{2\sqrt{c_1}}\right). \qquad (81)$$

Fig. 29 illustrates the distribution of elastic strains and hydrostatic stress in the plane y=0 near the line of the positive disclination located at the point (0,0) of Fig. 22 when d=$10^4\sqrt{c_k}$. The solid lines represent the gradient solution, while the dashed lines represent the classical one. One can see that in the gradient elasticity, the elastic strains and stresses are finite at the disclination line, they achieve extreme values there and tend to the classical solution far away from the disclination line.

Fig. 30 provides a general view on the distribution of elastic strains and stresses given by classical and gradient elasticity. The top pictures represent the classical solution, while the bottom pictures represent the gradient solution. Fig. 30 clearly demonstrates the elimination of classical singularities near the disclination line within the gradient theory.

The short-range elastic interaction between wedge disclinations may be illustrated by observing the dependence of the strained state at the line of one of the dipole disclinations on the dipole arm d. In doing so, one can use Eqs. 78 and 79 which are represented graphically in Fig. 31. It is seen that in the case of wedge disclinations, the elastic strains and hydrostatic stress vary monotonously with d, in contrast to the case of twist disclinations where they are non-monotonous for d<$10\sqrt{c_k}$. Here, only the strain component ε_{xx} achieves an extreme value at $d\approx\sqrt{c_2}$ but even this maximum has a small value. However, the strain and stress components are also zero at d=0 (annihilation of disclinations), as is the case with twist disclinations.

Another interesting feature when considering the short-range interaction between wedge disclinations is the transformation of the elastic fields of a dipole of wedge disclinations into the elastic fields of an edge dislocation when the dipole arm d becomes smaller than the scale unit $\sqrt{c_k}$. Fig. 32 shows the distribution of the strain components ε_{xx}, ε_{yy}, and ε (from top to bottom) for four subsequent positions of the negative wedge disclination ($-50\sqrt{c_2}$,0) – (a), ($-5\sqrt{c_2}$,0) – (b), ($-\sqrt{c_2}$,0) – (c), and ($-0.01\sqrt{c_2}$,0) – (d), while the positive wedge disclination occupies the same position (0,0). Again, the solid lines represent the gradient solution, while the dashed lines represent the classical one. We can see how the levels and profiles of the strain (stress) components are changing with decreasing d. The final pictures (Fig. 32d) give exactly the same strain distributions as we have reported in [60] for an edge dislocation (see Fig. 9). In our co-ordinate system, this dislocation would have a Burgers vector $-b_y$=$-\omega_z d$. This means that in the gradient elasticity, edge dislocations may be modelled through dipoles of wedge disclinations, as is the case in classical elasticity [5-7].

Thus, within the gradient theory of elasticity described by (5), dipoles of straight disclinations of general type give zero or finite values for the elastic strains and stresses at the disclination lines. The finite values depend strongly on the dipole arm d and show regular and monotonous (in the case of wedge disclinations) or nonmonotonous (in the case of twist disclinations) behavior for short-range (when d<$10\sqrt{c_k}$) interactions between disclinations. When the disclinations annihilate ($d\to 0$), the elastic strains and stresses tend regularly to zero values. Far from the disclination lines (r>>$10\sqrt{c_k}$), gradient and classical solutions coincide. When the dipole arm d is much smaller than the scale unit $\sqrt{c_k}$, the elastic fields of a dipole of wedge disclinations transform into the elastic fields of an edge dislocation, as is the case in classical elasticity.

5. CONCLUSIONS

Thus consideration of dislocations and disclinations within the gradient theory of elasticity described by (5) results in a complete eliminations of singularities from the elastic fields and energies of dislocations as well as from strains and stresses of disclinations at the defect lines. It has been shown that the elastic strains and stresses are strictly equal to zero at the dislocation lines and achieve their extreme values of ≈(3÷14)% and ≈(μ/4÷μ/2), respectively, at a distance ≈a/4 from the dislocation line. Two characteristic distances appear naturally in this approach: $r_0\approx 4\sqrt{c_2}$ which may be viewed as the radius of dislocation core and $d_0\approx 10\sqrt{c_2}$ which may be viewed as the radius of strong short-range interaction between dislocations. In considering dislocations near interfaces, it has been shown that all stress components remain continuous across the interface, in contrast to the well-known classical solution [69] where three (one for a screw dislocation and two for an edge dislocation) stress components suffer jump discontinuities there. Also, the classical singularity of the elastic "image" force acting upon the dislocation by the interface [69], is eliminated

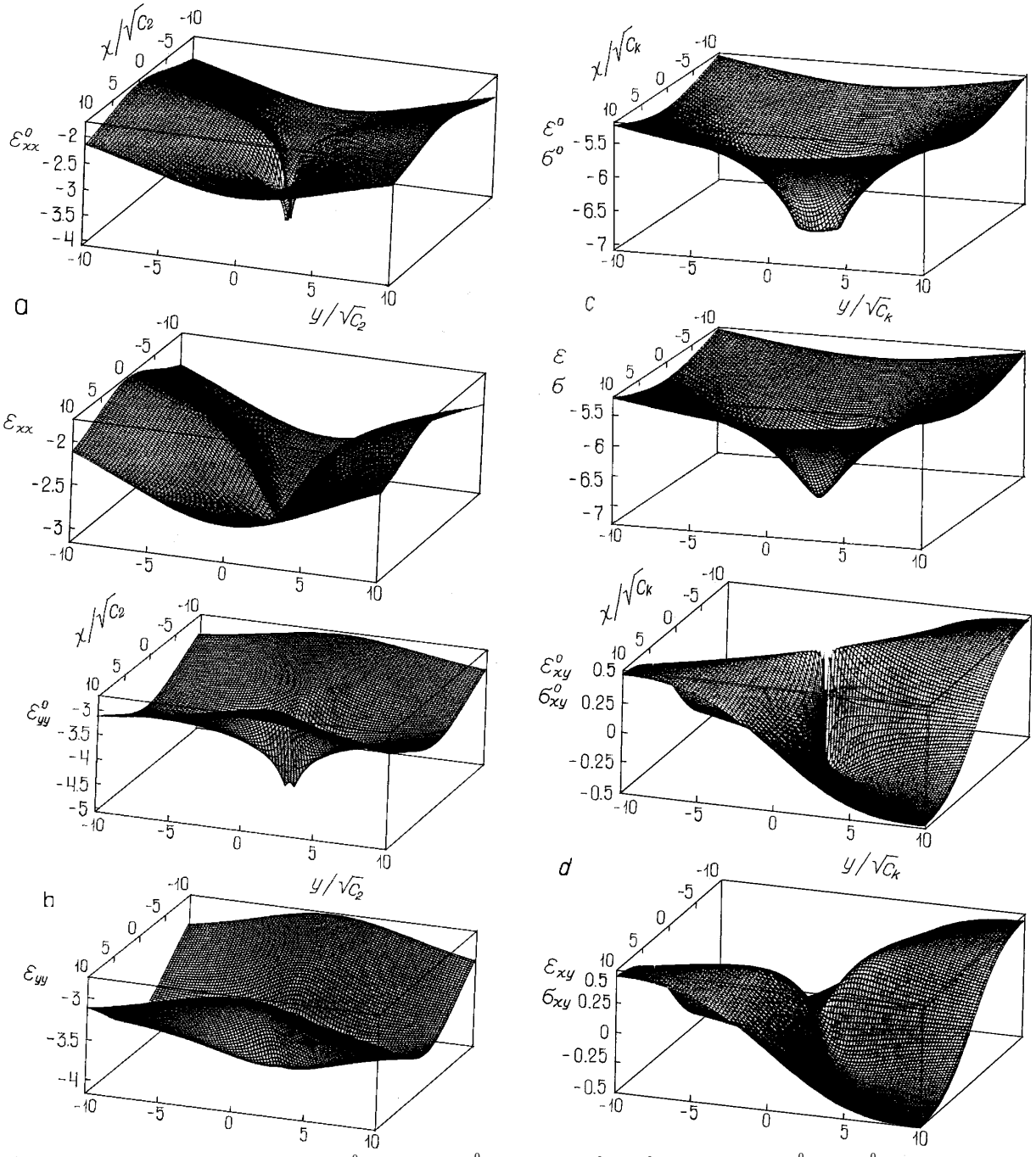

Fig. 30. The strain (stress) components ε^0_{xx}, ε_{xx} – (a), ε^0_{yy}, ε_{yy} – (b), ε^0, $\varepsilon(\sigma^0, \sigma)$ – (c), and ε^0_{xy}, $\varepsilon_{xy}(\sigma^0_{xy}, \sigma_{xy})$ – (d), near of the line of the positive wedge disclination when the dipole arm $d=10^4\sqrt{c_k}$. The strain values are given in units of $\omega_z/[4\pi(1-\nu)]$, while the stress values, in units of $\mu\omega_z(1+\nu)/[6\pi(1-\nu)(1-2\nu)]$ – (c), and $\mu\omega_z/[2\pi(1-\nu)]$ – (d). The top figures give the classical solution $\varepsilon^0_{ij}(\sigma^0_{ij})$ while the bottom ones give the gradient solution $\varepsilon_{ij}(\sigma_{ij})$.

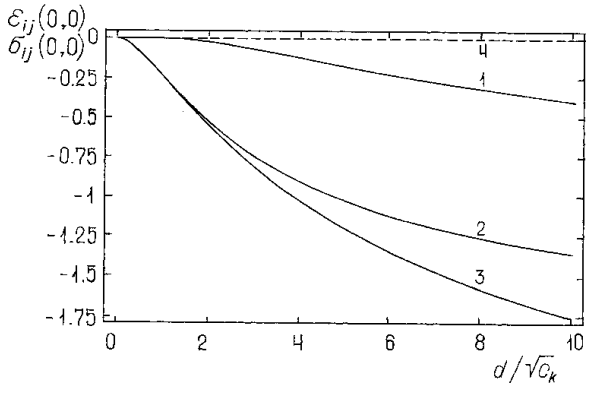

Fig. 31. The strain (stress) components ε_{xx} – (1), ε_{yy} – (2), $\varepsilon(\sigma)$ – (3), and $\varepsilon_{xy}(\sigma_{xy})=0$ – (4) at the line of the positive wedge disclination via the dipole arm d. The strain values are given in units of $\omega_z/[4\pi(1-\nu)]$, while the stress values, in units of $\mu\omega_z(1+\nu)/[6\pi(1-\nu)(1-2\nu)]$.

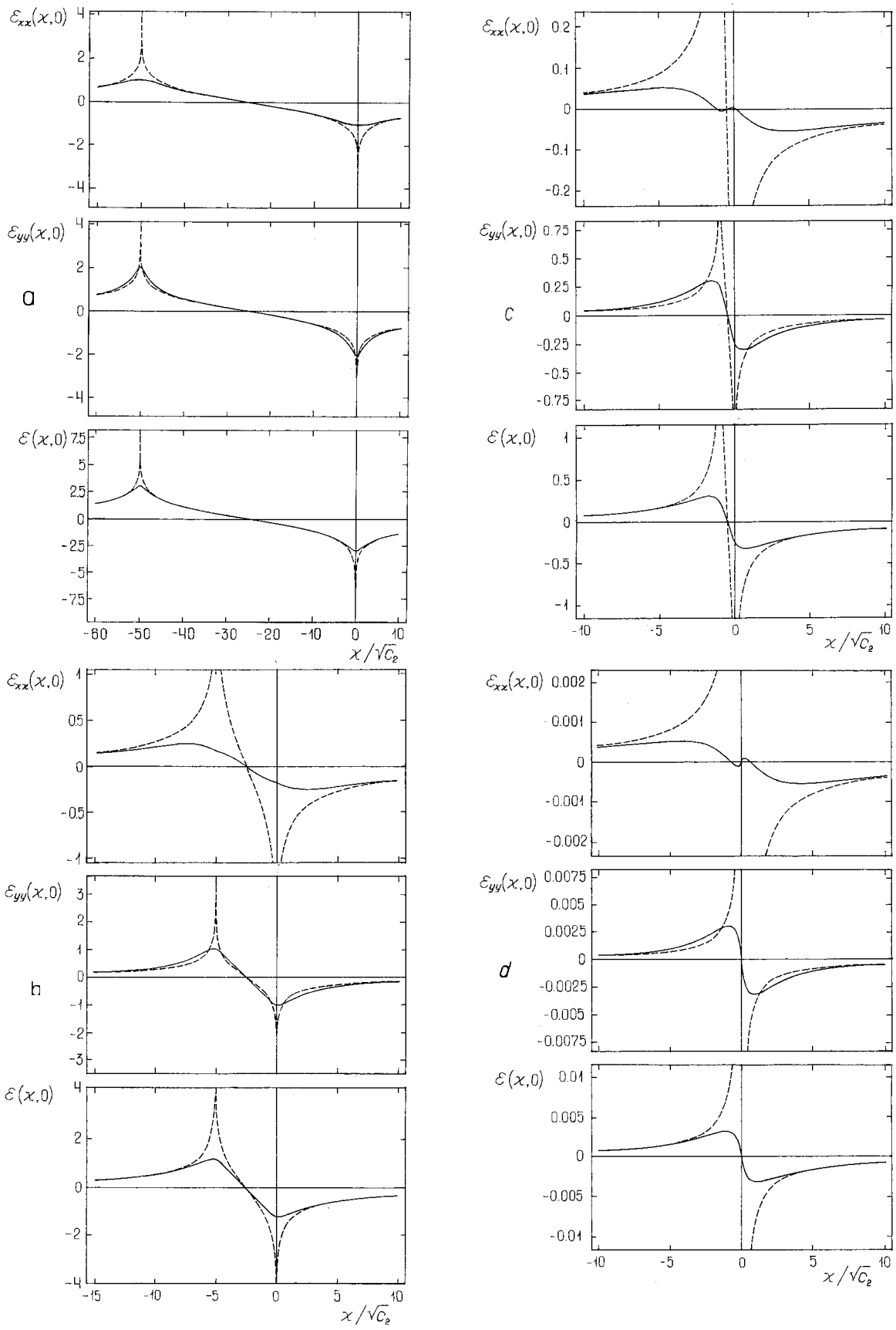

Fig. 32. The transformation of the strain components ε_{xx}, ε_{yy}, and ε (from top to bottom) of a dipole of wedge disclinations into those of an edge dislocation (d) having the Burgers vector $-b_y=-\omega_z d$, when the dipole arm d becomes smaller than the scale unit $\sqrt{c_2}$. The dipole arm d for four subsequent positions of the negative wedge disclination is equal to $50\sqrt{c_2}$ – (a), $5\sqrt{c_2}$ – (b), $\sqrt{c_2}$ – (c), and $0.01\sqrt{c_2}$ – (d). The strain values are given in units of $\omega_z/[4\pi(1-\nu)]$. The dashed curves represent the classical solution ε^0_{ij}.

from the gradient solution. The "image" force remains finite and continuous at the interface and has an additional short-range component due to the difference in the gradient coefficients of the media in contact. Under the action of this component, the screw (edge) dislocation tends to penetrate into the medium with the larger (smaller) gradient coefficient. In the general case where both the elastic constants μ_i and the gradient coefficients c_i are different for these media, the total "image" force exhibits quite different behavior near the interface depending on the ratios μ_2/μ_1 and c_2/c_1, while its long-range component remains as in the classical theory of elasticity. In considering disclination dipoles, one can conclude that non-vanishing at the disclination lines strains and stresses depend strongly on the dipole arm and tend regularly to zero values when the disclinations annihilate. In general, the gradient solutions permit one to calculate strains and stresses directly near a dislocation/disclination line and to analyze short-range interactions in dense ensembles of defects. The results reviewed can be of advantage when constructing physical models of the structure and mechanical behavior of metallic glasses and nanostructured materials as well as of conventional metals and alloys under large plastic deformations.

ACKNOWLEDGEMENTS

This work was supported by INTAS-93-3213/Ext and TMR/ERB FMRX CT 960062 and, in part, by the Volkswagen Foundation Research Project 05019225 and Russian Research Council "Physics of Solid-State Nanostructures" (Grant 97-3006). The author would like to thank Professor E.C. Aifantis and Dr. K.N. Mikaelyan for permanent collaboration, valuable contributions, fruitful discussions and encouragements.

REFERENCES

[1] J.P. Hirth and J. Lothe, *Theory of Dislocations* (John Wiley, New York, 1982).
[2] R. de Wit, In: *Fundamental Aspects of Dislocation Theory*, Vol. I, ed. by J. A. Simmons, R. de Wit and R. Bullough (Nat. Bur. Stand. (US), Spec. Publ. 317, 1970), p. 651.
[3] R. de Wit // *J. Res. Nat. Bur. Stand.* (U.S.) **77A** (1973) 49.
[4] R. de Wit // *J. Res. Nat. Bur. Stand.* (U.S.) **77A** (1973) 359.
[5] R. de Wit // *J. Res. Nat. Bur. Stand.* (U.S.) **77A** (1973) 608.
[6] V.A. Likhachev and R.Yu. Khairov, *Introduction to Disclination Theory* (Izdatelstvo LGU, Leningrad, 1975) (in Russian).
[7] A.E. Romanov and V.I. Vladimirov, In: *Dislocations in solids*, Vol. 9, ed. by F.R.N. Nabarro (North Holland, Amsterdam, 1992), p. 191.
[8] *Dislocations in solids*, Vols. 1-10, ed. by F.R.N. Nabarro (North Holland, Amsterdam, 1979-1996).
[9] V.V. Rybin, *Large Plastic Deformations of Metals* (Metallurgia, Moscow, 1986) (in Russian).
[10] V.G. Gryaznov and L.I. Trusov // *Progr. Mater. Sci.* **37** (1993) 290.
[11] A.P. Sutton and R. Balluffi, *Interfaces in Crystalline Materials* (Clarendon Press, Oxford, 1995).
[12] A.E. Romanov, In: *Nanostructured Materials: Science and Technology*, ed. by G.-M. Chow and N.I. Noskova (Kluwer, Dordrecht, 1998), p. 207.
[13] G.P. Cherepanov, *Mechanics of Brittle Fracture* (McGraw-Hill, New York, 1979).
[14] M.F. Kanninen and C.H. Popelar, *Advanced Fracture Mechanics* (Oxford University Press, New York, 1985).
[15] F.A. McClintock // *Acta Metal.* **8** (1960) 127.
[16] M. Mişicu // *Rev. Roum. Sci. Techn., Sér. méc. appl.* **10** (1965) 35.
[17] C. Teodosiu // *Rev. Roum. Sci. Techn., Sér. méc. appl.* **10** (1965) 1461.
[18] Z. Knésl and F. Semela // *Int. J. Eng. Sci.* **10** (1972) 83.
[19] J.P. Nowacki // *Bull. Acad. Polon. Sci., Sér. sci. techn*. **21** (1973) 585.
[20] J.P. Nowacki // *Bull. Acad. Polon. Sci., Sér. sci. techn*. **22** (1974) 379.
[21] W. Nowacki // *Arch. Mech.* **26** (1974) 3.
[22] S. Minagawa // *Letters in Appl. & Eng. Sci.* **5** (1977) 85.
[23] S. Minagawa // *Int. J. Eng. Sci.* **12** (1977) 447.
[24] J.P. Nowacki // *Arch. Mech.* **29** (1977) 531.
[25] L. Lejček // *Czech. J. Phys.* B **33** (1983) 447.
[26] L. Lejček // *Czech. J. Phys.* B **35** (1985) 655.
[27] L. Lejček // *Czech. J. Phys.* B **35** (1985) 726.
[28] L. Lejček and F. Kroupa // *Czech. J. Phys.* B **38** (1988) 302.
[29] R. Muki and E. Sternberg // *Z. Angew. Math. Phys.* **16** (1965) 611.
[30] E. Sternberg and R. Muki // *Int. J. Solids Structures* **3** (1967) 69.
[31] N.J. Pagano and G.C. Sih // *Int. J. Solids Structures* **4** (1968) 531.
[32] G.C. Sih and H. Liebowitz, *In: Fracture*, Vol. 2, ed. by H. Liebowitz, (Academic Press, New York and London, 1968), p. 175.

[33] E. Sternberg, *In: Mechanics of Generalized Continua*, ed. by E.Kröner (Springer-Verlag, Berlin-Heidelberg-New York, 1968), p. 95.
[34] G.R. Tiwari // *J. Indian. Math. Soc.* **34** (1970) 67.
[35] C. Atkinson and F.G. Leppington // *Int. J. Solids Structures* **13** (1977) 1103.
[36] N.F. Morozov, *Mathematical Questions of Crack Theory* (Nauka, Moscow, 1985) (in Russian).
[37] I.A. Kunin, *Theory of Elastic Media with Microstructure* (Springer, Berlin, 1986).
[38] A.D. Brailsford // *Phys. Rev.* **142** (1966) 383.
[39] A.C. Eringen // *J. Phys. D: Appl. Phys*. **10** (1977) 671.
[40] A.C. Eringen // *J. Appl. Phys.* **54** (1983) 4703.
[41] A.C. Eringen, *In: The Mechanics of Dislocations*, ed. by E.C. Aifantis and J.P. Hirth (American Society for Metals, Metals Park, Ohio, 1985), p. 101.
[42] K.L. Pan // *Radiat. Eff. Defects Solids* **133** (1995) 167.
[43] Y.Z. Povstenko // *J. Phys. D: Appl. Phys.* **28** (1995) 105.
[44] Y.Z. Povstenko // *Int. J. Engng. Sci.* **33** (1995) 575.
[45] Y.Z. Povstenko, In: *Proc. of Euromech-Mecamat, EMMC2: Mechanics of Materials with Intrinsic Length Scale*, ed. by A. Bertram et al, (Magdeburg, 1998), p. 299.
[46] A.C. Eringen, C.G. Speziale and B.S. Kim // *J. Mech. Phys. Solids* **25** (1977) 339.
[47] N. Ari and A.C. Eringen // *Cryst. Lattice Defects Amorph. Mat.* **10** (1983) 33.
[48] B.S. Altan and E.C. Aifantis // *Scripta Metall. Mater*. **26** (1992) 319.
[49] C.Q. Ru and E.C. Aifantis // *Acta Mechanica* **101** (1993) 59.
[50] E.C. Aifantis // *J. Mech. Behaviour of Materials* **5** (1994) 355.
[51] D.J. Unger and E.C. Aifantis // *Int. J. Fracture* **71** (1995) R27.
[52] G.E. Exadaktylos and E.C. Aifantis // *J. Mech. Behavior of Materials* **7** (1996) 93.
[53] I. Vardoulakis, G. Exadaktylos and E.C. Aifantis // Int. J. Solids Structures **33** (1996) 4531.
[54] B.S. Altan and E.C. Aifantis // *J. Mech. Behavior of Materials* **8** (1997) 231.
[55] C.Q. Ru and E.C. Aifantis, *Preprint* (MTU Report, Houghton, MI, 1993).
[56] W.W. Milligan, S.A. Hackney and E.C. Aifantis. *In: Continuum Models for Materials with Microstructure*, ed. by H. Mühlhaus (Wiley, 1995), p. 379.
[57] R.D. Mindlin // *Int. J. Solids Structures* **1** (1965) 417.
[58] M.Yu. Gutkin and E.C. Aifantis // *Phys. Stat. Sol.* (b) **214** (1999) 245.
[59] M.Yu. Gutkin and E.C. Aifantis // *Scripta Mater.* **35** (1996) 1353.
[60] M.Yu. Gutkin and E.C. Aifantis // *Scripta Mater.* **36** (1997) 129.
[61] M.Yu. Gutkin and E.C. Aifantis // *Scripta Mater.* **40** (1999) 559.
[62] M.Yu. Gutkin and E.C. Aifantis, *In: Nanostructured Films and Coatings*, ed. by Y. Tsakalakos and I.A. Ovid'ko (Kluwer, Dordrecht, 2000).
[63] M.Yu. Gutkin and E.C. Aifantis // *Phys. Solid State* **41** (1999) 1980.
[64] M.Yu. Gutkin, K.N. Mikaelyan and E.C. Aifantis // *Phys. Solid State* **42** (2000) No. 8.
[65] M.Yu. Gutkin, K.N. Mikaelyan and E.C. Aifantis // *Scripta Mater.* **42** (2000).
[66] K.N. Mikaelyan, M.Yu. Gutkin and E.C. Aifantis // *Phys. Solid State* **42** (2000) No. 9.
[67] G. Gutekunst, J. Mayer and M. Rühle // *Mater. Sci. Forum* **207-209** (1996) 241.
[68] P.C. Gehlen, A.R. Rosenfield and G.T. Hahn // *J. Appl. Phys*. **39** (1968) 5246.
[69] T. Mura, *In: Advances in Materials Research*, ed. by H. Herman, Vol. 3 (Interscience Publishers, New York/London/Sydney/Toronto, 1968), p. 1.
[70] J.D. Eshelby, *In: Dislocations in Solids*, ed. by F.R.N. Nabarro, Vol. 1 (North-Holland, Amsterdam, 1979), p. 167.
[71] M.Yu. Gutkin and A.E. Romanov // *Phys. stat. sol.* (*a*) **125** (1991) 107.
[72] M.Yu. Gutkin, A.L. Kolesnikova and A.E. Romanov // *Mater. Sci. Engng.* A **164** (1993) 433.
[73] R. Bonnet // *Phys. Rev.* B **53** (1996) 10978.